Structural Analysis of Mechanism and Regulation of Glutamine Amidotransferases.

by
Amber Marie Smith

A dissertation submitted in partial fulfillment
of the requirements for the degree of
Doctor of Philosophy
(Biological Chemistry)
in the University of Michigan
2014

Doctoral Committee:

Professor Janet L. Smith, Chair
Professor John J. Tesmer
Associate Professor Raymond C. Trievel
Associate Professor Georgios Skiniotis
Professor William L. Smith

For my mother, grandmother and great grandmother.

Acknowledgments

A thesis would not be complete without acknowledgement of all the people that made it possible. First and foremost, I would like to express the deepest appreciation to my mentor, Professor Janet Smith. Not only has Janet been supportive in my scientific career, but in my personal life as well. She is an amazing role model and is an example of the dedication and persistence necessary to be a successful scientist. Without her guidance and support, none of this would have been possible.

I would also like to thank my thesis committee members Professor John Tesmer, Professor Georgios Skiniotis, Professor Ray Trievel and Professor William Smith. It has been an honor to be surrounded by such gifted and passionate scientists; I know that I am better off because of it. Their suggestions, guidance, and support throughout this entire process left me feeling as if I have not only one, but multiple mentors.

In addition, a big thank you is due to all the members of the Smith lab. I am so grateful for their constant support and camaraderie which has made this whole process possible, and more importantly, fun. Our lab definitely felt like a home away from home. I especially want to thank David Akey for all of his support, suggestions, edits, excitement (over new results) and confidence in my ability. I also want to thank Jon Whicher and Steffen Bernard, both of which will be lifelong friends. I thank them for sharing their journey with me and participating in mine.

Finally, I would like to thank my family and friends. Without their love and support I would not have been able to move across the country in pursuit of my dreams. And to my life partner, without your support this journey would have been lonely.

Table of Contents

List of Figures

List of Tables

Abstract

Glutamine amidotransferases (GATs) use glutamine as a nitrogen source for a diverse array of biosynthetic processes. GATs hydrolyze glutamine in a glutaminase domain and transfer ammonia to various acceptor substrates in a synthase domain. Allosteric regulation plays a large role in the mechanisms of GATs. Substrate binding induces structural changes to both the synthase and glutaminase domains, contributing to product formation. Capturing these structural changes is a challenge in understanding the mechanisms of GATs. This thesis investigates two different GATs: pyridoxal 5'-phosphate synthase (PLPS) from the bacterium *Geobacillus stearothemophilus* and cytosine triphosphate synthetase (CTPS) from the bacterium *Aquifex aeolicus.*

PLPS generates pyridoxal 5'-phosphate (PLP) from glutamine, ribose 5-phosphate (R5P) and glyceraldehyde 3-phosphate (G3P). The mechanism of PLP formation was probed by solving crystal structures in three distinct states that capture two covalent intermediates of the synthase active site and one of the glutaminase active site. The structures reveal a complex set of conformational changes that sequester the active sites from bulk solvent. Key roles were identified for several charged amino acids.

CTPS converts uridine triphosphate (UTP) to cytosine triphosphate (CTP) through ATP-activated amination of UTP. GTP serves as an allosteric activator of CTPS, increasing glutaminase activity 3-4 fold when glutamine is the nitrogen source. To

investigate the GTP binding site I used X-ray crystallography, negative-stain electron microscopy and binding experiments to monitor the structural changes induced by GTP. The basis for CTPS inhibition by excessive GTP was established.

Chapter 1

Introduction

Glutamine Amidotransferases

The glutamine amide group is a major source of nitrogen for the biosynthesis of amino acids, purine and pyrimidine nucleotides, amino sugars, and coenzymes as it is transferred to acceptor substrates in a variety of biosynthetic pathways[1]. Glutamine amidotransferases (GATs) are responsible for sequestering, transferring and incorporating nitrogen from glutamine to a variety of products. GATs are a diverse group of enzymes that have two active sites: a glutaminase active site hydrolyzes glutamine to ammonia, and glutamic acid and a synthase active site (synthetase, in the case where ATP activation is required) where ammonia is combined with acceptor substrates to generate a product (Fig. 1.1)[1,2]. While ammonia alone can serve as the nitrogen donor for most GATs, ammonia is less effective than glutamine as a nitrogen source[1].

Utilizing glutamine not only provides an amino group for a variety of biosynthesis pathways, but also links carbon and nitrogen metabolism[3]. Glutamine synthetase is responsible for the condensation of ammonia and glutamate and is the only enzyme that incorporates ammonium ions into organic compounds. Additionally, glutamate can be converted to α-ketoglutarate, a key intermediate in the Krebs cycle, through oxidative deamination using glutamate dehydrogenase. These anaplerotic reactions replenish the Krebs cycle reserve of α-ketoglutarate, regulate the concentration of the cell's favored

nitrogen source (glutamine), and balance the cell's amino acid pools. Regulating α-ketoglutarate levels plays a role in extending lifespan and delaying ageing in *Caenorhabditis elegans*[4].

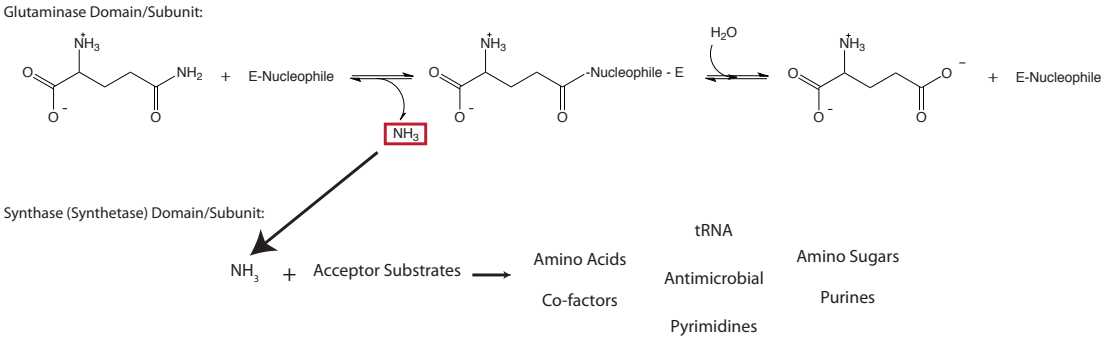

Figure 1.1 Simplified scheme of the overall GAT reaction and the known products produced by GATs.

The bi-enzyme functionality of GATs is accommodated through multiple domains on a single polypeptide or separate interacting subunits. Channeling is an absolute requirement for GATs due to the lability of NH_3 and the distance between their distinct active sites, which ranges from 10 Å to 40 Å [5]. This range is due to the variation in architecture among GATs. The mode for opening and closing the channel and the specific path of ammonia transfer for most GATs has been left to speculation due to the limits of structural analysis. In addition to ensuring the arrival of ammonia at the synthase active site, the channel from the glutaminase active site to the synthase active site must protect the ammonia from conversion to non-reactive ammonium ion[5].

Allosteric regulation plays a large role in the mechanisms of GATs[6,7]. GATs require synchronization of the glutaminase and synthase active sites to ensure that all substrates are consumed at the same rate. The accepted paradigm for this regulation is

that glutaminase activity is dependent on the presence of synthase substrates or the formation of the intact protein[1,8]. To achieve this level of regulation, GATs have a defined order of substrate binding. Deciphering the mechanism behind this order is therefore imperative to understanding how the products are formed[6,7]. Additionally, substrate binding plays a large role in regulation: as each substrate binds to the enzyme, the structures of both the synthase and glutaminase domains experience conformational changes that contribute to catalysis[6,7,9]. Capturing these structural changes is the most challenging aspect of understanding the mechanisms of GATs.

GAT Classifications:

GATs are categorized exclusively by their glutaminase domain, which belong to four different groups: Triad GATs (class I), N-terminal nucleophile (Ntn) GATs (class II), amidases, and nitrilases (Table 1.1). These classifications are based on their catalytic residues and motifs, protein folds, and the way they recognize glutamine[1,10,11]. Triad GATs and Ntn GATs encompass most of the GATs studied thus far. The amidase and nitrilase groups each contain only one known GAT. The synthase domain, mechanism of ammonia incorporation and final product from each GAT are diverse[1,2].

Class I: Triad GATs.

Triad GATs are characterized by an α/β fold and three invariant catalytic residues: cysteine, histidine and glutamate[10]. The catalytic triad, located at one end of the core β-sheet of the glutaminase domain, drives glutamine hydrolysis in a mechanism very similar to serine or cysteine proteases[10]. The α/β fold of these proteins is that of α/β hydrolyses with the characteristic feature of a tight α/β connection, also

known as the 'nucleophile elbow' with the cysteine nucleophile lying at the elbow junction[10]. The nucleophilic cysteine is part of a Gly-Xaa-Cys-Xaa-Gly motif while the catalytic His and Glu are part of a His-Pro-Glu motif[1]. The backbone nitrogens of the residue immediately following the nucleophilic cysteine and a residue located on an adjacent β-strand constitute an oxyanion hole that helps to stabilize the negative charge on the tetrahedral intermediate[5]. The domain architecture of Triad GATs is highly variable. The glutaminase and synthase domains can be either on one polypeptide, or on interacting subunits[1]. When contained on one polypeptide, the domain order varies[1].

Class II: N-terminal nucleophile (Ntn) GATs.

Ntn GATs are part of the Ntn hydrolase superfamily that catalyzes a diverse range of hydrolytic reactions[11,12]. The glutaminase and synthase domains are invariably located on a single polypeptide with the glutaminase domain located at the N-terminus[1]. Ntns have a cysteine nucleophile as the first amino acid of the mature enzyme and share a similar α/β core structure comprised mainly of antiparallel β-strands[5,11,12]. The oxyanion hole for the tetrahedral intermediate is stabilized by the conserved residues Asn and Gly that are adjacent in sequence[1].

Table 1:1 List of GAT classifications and examples.

Glutaminase Family	Protein	Domains or Subunits	Oligomeric State	Catalytic Residues	Glutaminase Fold	Oxyanion Hole
Triad	GMP synthetase	Domains	Homodimeric	His, Cys, Glu	α/β fold	Gly, Tyr
	Anthranilate synthase	Subunits	Heterotetramer			Gly, Leu
	Aminodeoxychorismate synthase	Subunits	Heterodimeric			
	Imidazole glycerol phosphate synthase	Domains/ Subunits	Heterodimeric/ Monomer			Gly
	Carbamyl phosphate synthetase	Subunits	Heterodimeric			Gly, Leu
	CTP synthetase	Domains	Homotetramer			Gly, Leu
	Formylglycinamidine synthetase	Domains/ Subunits	Monomer/ Heterotrimer			Gly, Ser
	Cobyrinic and cobyric acid synthetases	Domains	Monomer			
	PLP synthase	Subunits	Hetero-24-mer			Gly, Ala
N-terminal	Glutamine PRPP amidotransferase	Domains	Homotetramer	N-terminal Cys	α/β fold (mainly antiparallel β-sheets)	Asn, Gly
	Glucosamine-6-phosphate synthase		Homodimer			
	Glutamate synthase		Monomer			
	Asaparagine synthetase		Homodimer			
Nitrilase	NAD^+ synthetase	Domains	Homo-8-mer	Glu, Lys, Cys	αββα sandwich	Lys
Amidase	Glu $tRNA^{Gln}$ amidotransferase	Subunits	Heterotrimer	Ser, *cis*Ser, Lys	β-sandwich surrounded by α-helices	Thr, Gly, Ser

Amidases and nitriliases.

The amidase and nitriliase GAT families each include only one GAT. Most of the members of the amidase family hydrolyze aliphatic amides and are distinguished from other hydrolases by a Ser-*cis*Ser-Lys catalytic triad and a distinct fold[13,14]. Amidases also contain a “GGSS motif” of ~130 amino acids that is glycine-, alanine- and serine-rich, also known as the amidase signature[14-16]. GatCAB is the only example of an amidase GAT. GatCAB is a heterotrimeric enzyme containing an amidase glutaminase subunit (GatA), a synthetase subunit (GatB) and a structural subunit (GatC)[17,18]. GatCAB is responsible for converting the incorrectly acylated bacterial tRNAs (Glu-$tRNA^{Gln}$ and Asp-$tRNA^{Asn}$) to the cognate one by amidating the misacylated tRNA substrate.

Found in both prokaryotes and eukaryotes, NAD^+ synthetase is the only known example of a GAT in the nitrilase family[19]. The glutaminase domain and synthetase

domain are located on the same polypeptide for this GAT class[20]. The N-terminal glutaminase domain is comprised of a central β-sandwich surrounded by α-helices[21]. Proteins within this family share a conserved Glu-Lys-Cys catalytic triad[19,21].

GATs are important examples of enzymes that employ two active sites to catalyze a two-step biochemical reaction. The activities of GATs span many facets of biosynthesis, contributing to the vast differences among the GATs and the increasing interest in this group of enzymes. These differences include their synthase domains/subunits, oligomeric state/architecture, substrates, mechanisms and final products. Structural studies have proved to be imperative in providing insights into how GATs function and have exposed the importance of structure to the function of each GAT. Surprisingly, these insights revealed similarities across different pathways and demonstrated how structure is essential to understanding the mechanism for each GAT.

Crystallography allows researchers to examine the complexity of these bi-catalytic proteins, further clarifying the large role that allosteric regulation plays in their function[1]. Due to the complexity of multi-step catalysis, it is difficult to obtain the entire picture of the overall reaction from a single structure model. Therefore multiple “snap shots” of these proteins with different combinations of bound substrates are the most effective way to understand the overall mechanism behind these synchronized complexes. My thesis project has been to take an in depth look into two different Triad GATs: pyridoxal 5’-phosphate synthase (PLPS) from the bacterium *Geobacillus stearothemophilus* and cytosine triphosphate synthetase (CTPS) from the hyperthermophilic bacterium *Aquifex aeolicus.*

Pyridoxal 5'-Phosphate Synthase

PLP

Vitamin b_6 consists of three different vitamers: pyridoxal, pyridoxamine and pyridoxine (Fig. 1.2). The overall structure of each of these vitamers includes a core pyridine ring containing 2-methyl, 3-hydroxyl and 5-hydroxymethyl substituents. The substituent at the 4' position differs among the three vitamers. To be converted into its biologically active form, each vitamer is phosphorylated at the hydroxymethyl. The carbaldehyde at the 4' of pyridoxal 5'-phosphate (PLP) is responsible for its ability to bind to both enzyme (through a Schiff base) and substrate to stabilize reaction intermediates. Stabilization occurs through the extremely efficient ability of PLP to absorb or delocalize the excess electron density on a deprotonated reaction intermediate (Fig. 1.3).

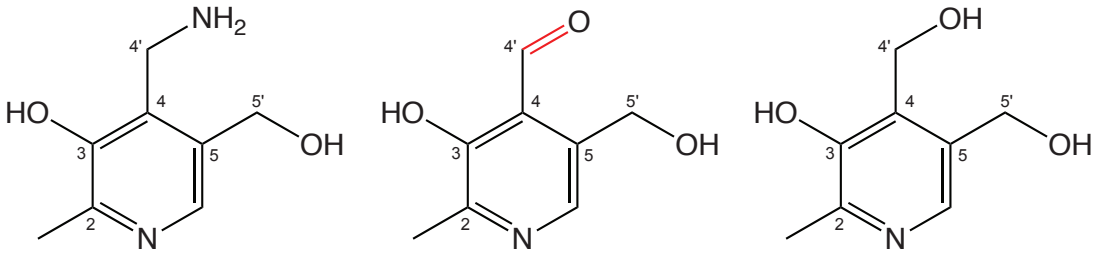

Pyridoxamine **Pyridoxal** **Pyridoxine**

Figure 1.2 The three vitamin b_6 vitamers. The substituent at the 4' position determines the biological activity of each vitamer. The aldehyde of pyridoxal gives this vitamer the highest biological activity (red).

PLP-dependent enzymes participate in reactions involved in amino acid metabolism, gluconeogenesis and lipid metabolism[22-24]. It is estimated that 1.5% of prokaryotic genes encode for PLP dependent enzymes, prompting the interest in targeting the prokaryotic PLP biosynthetic pathway as a mode for generating antibiotics and/or antifungals[25,26]. PLP-catalyzed reactions include: transamination, decarboxylation, racemization, elimination or replacement of an electrophilic group, and phosphorolysis[23,27].

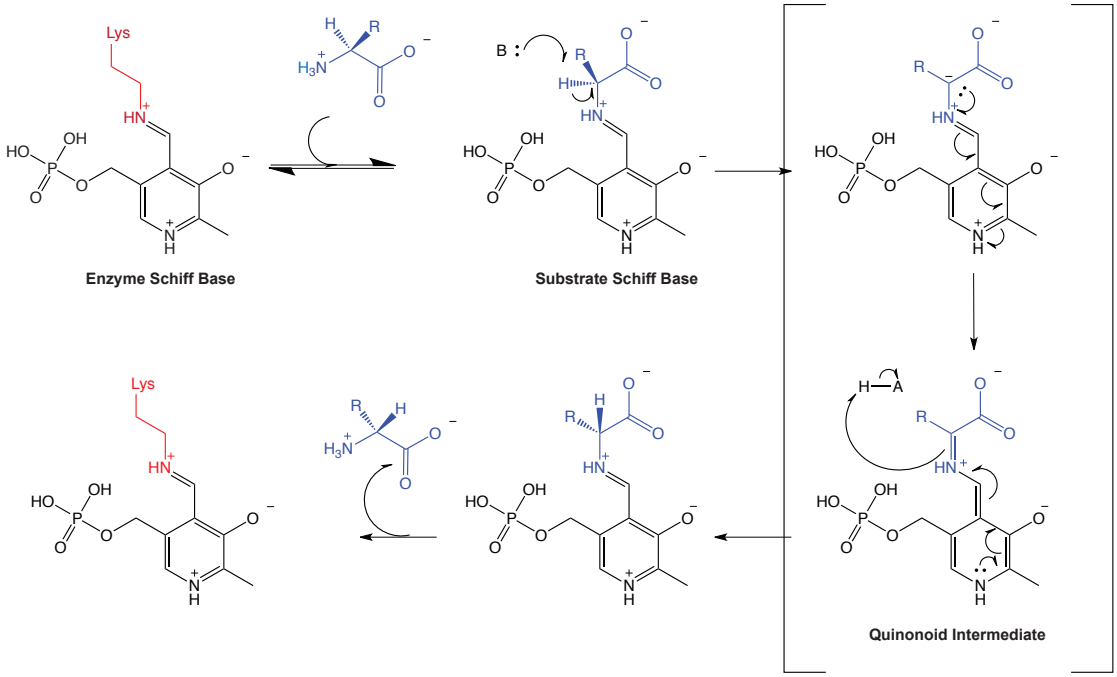

Figure 1.3: Example of PLP as an electron sink, stabilizing intermediates for a racemase reaction.

In addition to its role as a co-factor, PLP also exhibits antioxidant properties, as it can quench singlet oxygen radicals through its pyridine ring and hydroxyl and amine substituents[28-30]. The antioxidant properties of PLP make the PLP biosynthetic pathway essential to the fungus *Cercospora nicotianae,* the plant pathogen producer of cercosporin, a photo-activated toxin[29,31]. The resistance of the fungus to cercosporin,

which is necessary for its pathogenicity, is dependent on its ability to generate PLP[32]. Therefore, targeting the PLP biosynthetic pathway in fungi provides a potential antifungal. Overall, understanding the role of PLP in nature and the biosynthetic pathway responsible for its generation is key to taking advantage of all the potential antibiotic and antifungal properties.

De Novo PLP Biosynthetic Pathways

Two *de novo* pathways exist for the generation of PLP, the deoxyxylulose 5-phosphate (DXP) dependent pathway and the DXP-independent pathway (Fig. 1.4). The DXP-dependent pathway was the first pathway identified and has been studied extensively. Discovered in *Escherichia coli,* this pathway consists of two branches and seven enzymatic steps[33]. The substrates for this pathway are D-erythrose 4-phosphate (pentose phosphate pathway), glyceraldehyde 3-phosphate (glycolysis) and pyruvate (glycolysis)[33]. This pathway is found only in gamma proteobacteria, and, despite the original speculation, is not the most common pathway for PLP biosynthesis[31].

The DXP-independent pathway was identified indirectly. Originally thought to be predominately involved in fungal resistance to photosensitizing toxins, it was later revealed that the gene, *PDX1*, responsible for this phenotype is conserved in all domains of life (bacteria, archaea, eukarya) and is involved in PLP synthesis[31-33]. This led to the discovery of a second linked gene involved in this “novel” PLP biosynthetic pathway, named *PDX2*[34,35]. Sequence alignments classified this protein (Pdx2) to the family of Triad GATs[32]. It was also determined that the nitrogen found in PLP is derived from glutamine, consistent with the involvement of a GAT family enzyme[34,36,37]. Ribose 5-phosphate (R5P) and glyceraldehyde 3-phsophate (G3P) were identified as the

synthase acceptor substrates[38-40]. This “novel” PLP biosynthetic route is interesting due to its simplicity of one enzyme and three readily available substrates, which are common to the primary metabolism of the cell. These characteristics are thought to be the reason why the DXP-independent pathway is more widespread than the DXP-dependent pathway.

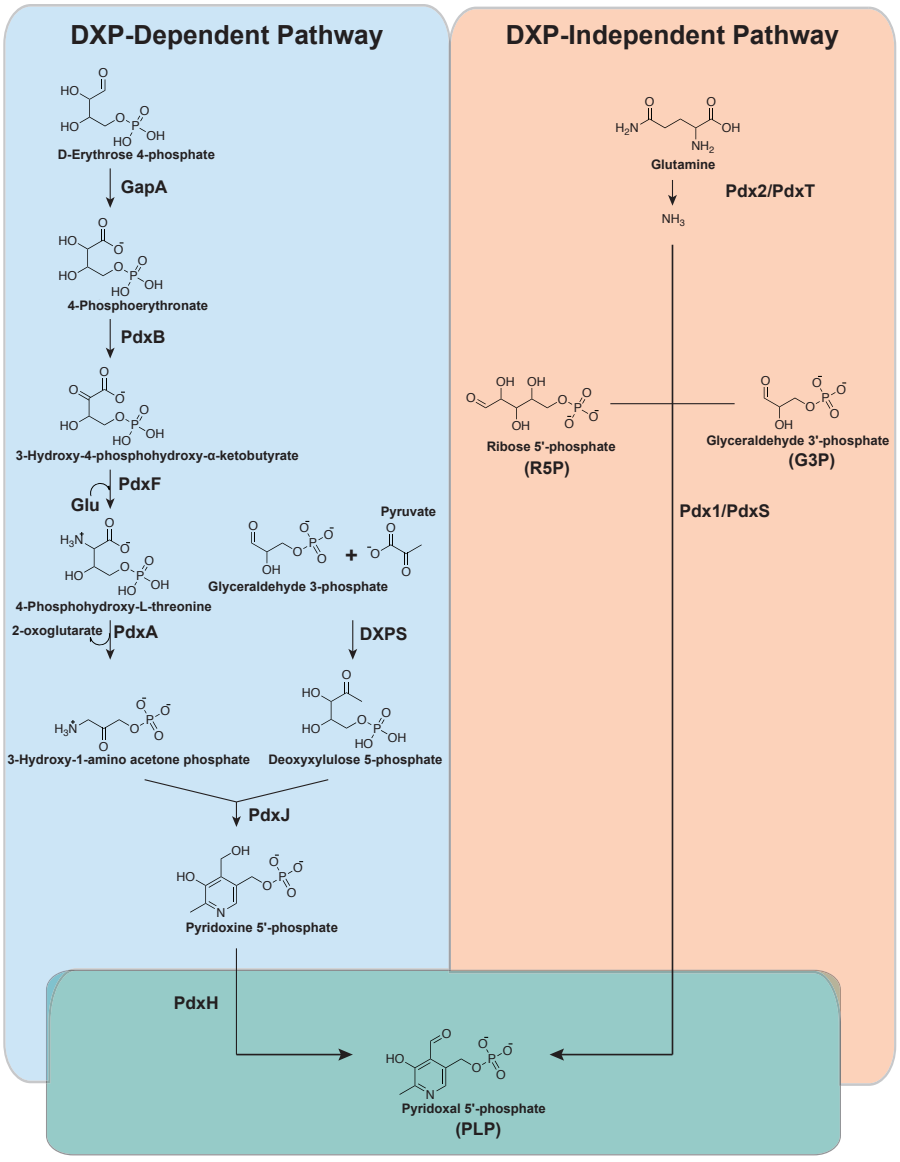

Figure 1.4: The two pathways of pyridoxal 5'-phosphate (PLP) biosynthesis[33].

PLPS

Homologs of the Pdx1 synthase and Pdx2 glutaminase from many organisms have been identified and reconstituted[31,35,41-46]. Pdx1 (*Bacillus subtilis)* homologs include YaaD (*Thermotoga maritima)*, Snz1 (*Saccharomyces cerevisiae)* and PdxS

(*Geobacillus stearothermophilus),* and Pdx2 (*B. subtilis)* homologs include YaaE (*T. maritima)*, Sno1 (*S. cerevisiae)* and PdxT (*G. stearothermophilus)*. This thesis concerns PLPS from *G. stearothermophilus* and the PdxS/PdxT nomenclature and amino acid sequence numbering will be used throughout. The structure of the intact PLPS enzyme is well understood and conserved among homologs[9,47-51]. Pyridoxal 5'-phosphate synthase (PLPS) is a D_6-symmetric complex of 12 synthase subunits (PdxS; 32kDa) and 12 glutaminase subunits (PdxT; 25kDa) (Fig.1.5). PdxS forms a cylindrical dodecamer of two opposing interdigitating hexameric rings that stack to give the overall shape of a barrel[48]. Each monomer of PdxS possesses the classic $(\beta/\alpha)_8$ barrel fold consisting of 8 parallel β-strands that alternate with 8 α-helices[48]. PdxS contains a handful of modification helices that are non-canonical to the $(\beta/\alpha)_8$ barrel fold, that either participate in the interactions with adjacent monomers or decorate the C-terminal side of the $(\beta/\alpha)_8$ barrel fold. The overall architecture of the D_6 PdxS core is a barrel of perpendicular barrels. PdxS structures have been reported from *B. subtilis*[9], *S. cerevisiae*[50], *T. maritima*[49], *G. stearothermophilus*[48] and *P. falciparium*[51]. A C-terminal tail of 14-28 amino acids is disordered in all the structures. PdxT binds to PdxS in a 1:1 ratio in which 12 PdxT subunits surround the PdxS stacked rings like studs, each interacting with one PdxS partner[48]. PdxT binds to the N-terminal side of the $(\beta/\alpha)_8$ barrel fold of PdxS.

PdxT has the classic α/β fold of a Triad glutaminase domain[1,47,52]. The core of PdxT is made up of a central 7-stranded β-sheet that is predominantly parallel[47]. The central β-sheet is sandwiched between six helices and two small β-sheets: one sheet

contains two parallel adjacent strands and one anti-parallel β-strands, while on the other side of the central β-sheet lies two antiparallel β-strands[47,52].

PdxS and PdxT carry out the synthase and glutaminase reactions, respectively[8]. PdxT is responsible for glutamine hydrolysis, which is carried out by the conserved catalytic triad (Cys78, His169 and Glu171) and the conserved oxyanion hole (Gly46 and Ala79)[9]. Structural rearrangements facilitated by PdxS-PdxT complex formation and the presence of glutamine lead to a peptide flip between residues Gly45 and Gly46, allowing the Gly45 amide to form the oxyanion hole[9]. This explains why PdxT lacks glutaminase activity in the absence of PdxS[53]. Unlike any other GAT studied to date, PLPS glutaminase activity is not dependent on the presence of the synthase substrates; it is contingent only on formation of the intact enzyme[8]. The ammonia generated by PdxT is channeled to PdxS where it is combined with R5P and G3P to generate PLP[8,40]. The synthase activity is significantly more efficient when glutamine is the nitrogen source[54,55].

In spite of the overall simplicity of the DXP-independent pathway, the mechanism of PdxS is elusive and largely unknown. Understanding substrate order and the intermediates formed throughout the reaction is imperative in attempting to dissect the mechanism of PdxS. PdxS catalyzes a complicated and fascinating set of reactions to form PLP from three substrates, R5P, NH_3 and G3P. The first synthase intermediate discovered was a covalent attachment between R5P and an active site lysine concomitant with the loss of water[40]. The identity of the modified lysine was controversial. Initially the covalent adduct was detected on Lys149 by peptide analysis using MS-MS, but the first structure of PLPS co-crystallized with R5P revealed the

attachment at Lys81[40,49]. Both lysines are invariant. Initially believed to be an imine between the active site lysine and R5P, it was identified through ^{13}C labeling and 1-dimensional NMR experiments that R5P is attached through C1 to the lysine as an amino ketone (Fig. 1.6)[56].

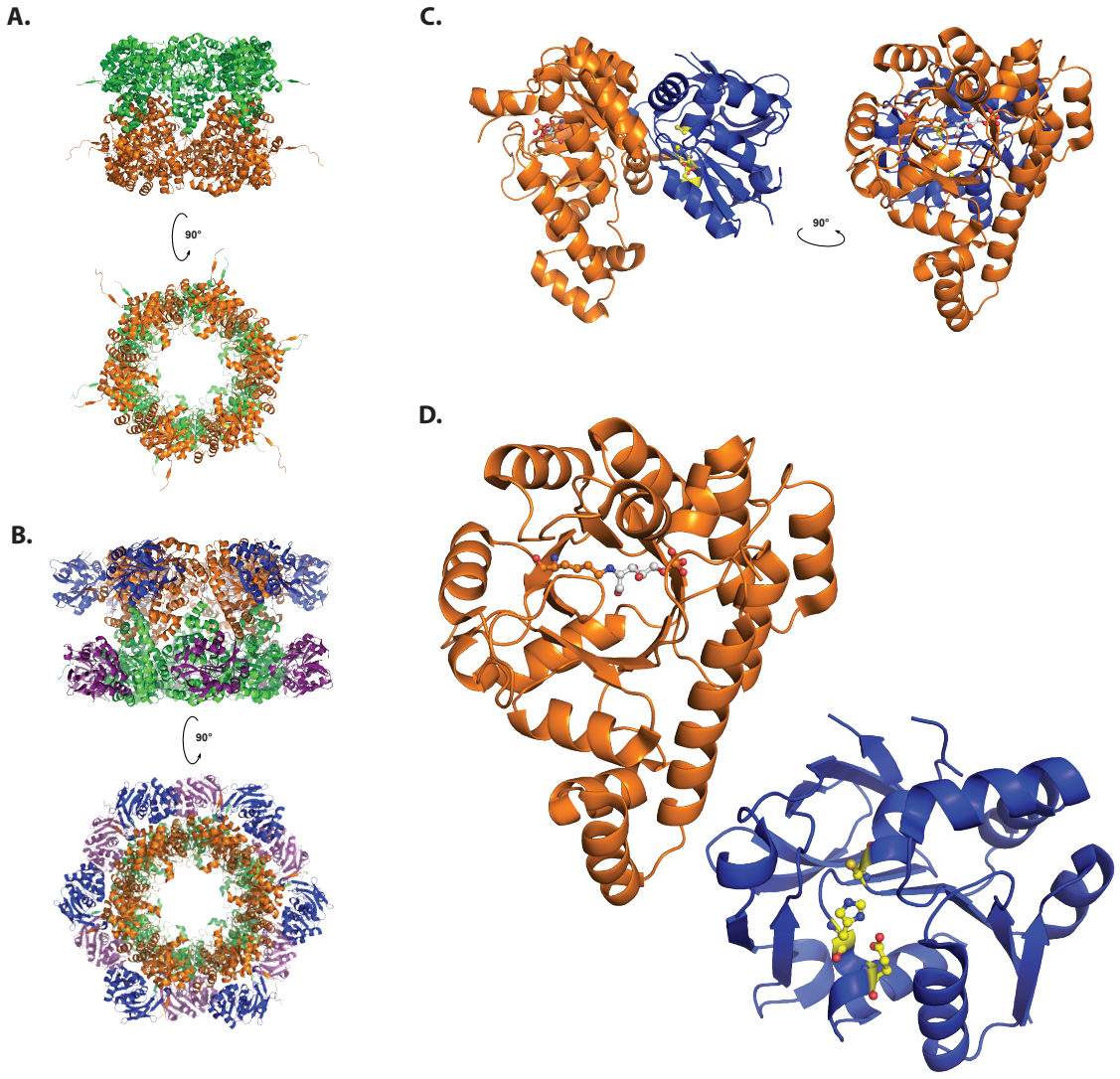

Figure 1.5 Organization of PLPS 24-mer A. The synthase subunit (PDB: 2ISS, *T. maritima*; orange and green) of PLPS forms a cylindrical dodecamer. B. The glutaminase subunit (blue and purple) binds to the synthase subunit (orange and green) like studs. C. The catalytic protomer includes one synthase monomer (orange) and one glutaminase monomer (blue). D. Lys81 in the synthase subunit is the site of Schiff base formation with R5P (Lys81; orange ball-and-stick, R5P; gray ball-and-stick). The glutaminase catalytic triad consists of a Cys78, His169 and Glu171 (yellow ball-and-stick).

Further investigation led to the discovery of a second covalent intermediate on the path to PLP[55]. Formation of this chromophoric intermediate is dependent on the presence of R5P and ammonia[55]. Analysis of this new intermediate determined a strong

UV absorption at 315 nm. Biochemical assays and mass spectrometry revealed that the chromophoric adduct is generated after the amino ketone has undergone dehydration, loss of inorganic phosphate and incorporation of ammonia[54-57]. Additionally, chromophore formation requires the C-terminal 30 amino acids of the synthase subunit, which are disordered in all published structures[6]. Where G3P binds to the synthase subunit, how G3P combines with the chromophore adduct and why the C-terminal tail of the synthase subunit is crucial to function are essential missing pieces from the puzzle in understanding the overall mechanism of PdxS.

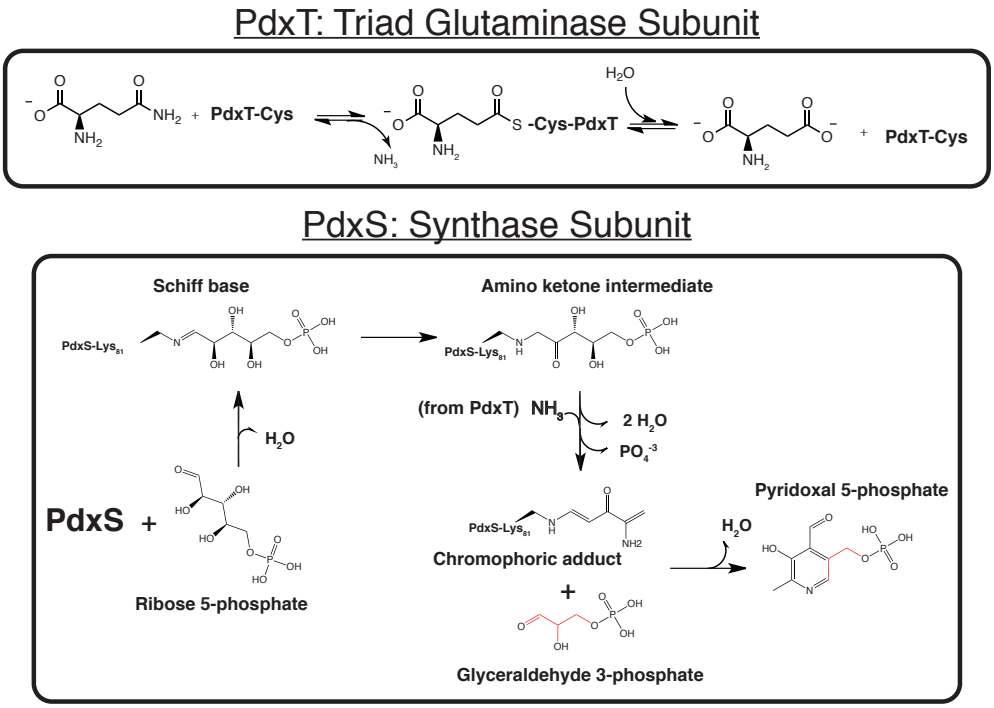

Figure 1.6 PLP biosynthesis catalyzed by PLPS. Ammonia generated by glutamine hydrolysis in PdxT is channeled to the PdxS active site where it joins R5P and G3P to form PLP by an unknown mechanism that proceeds through two sequential covalent intermediates. First, R5P and PdxS (Lys81) form a Schiff base that isomerizes to a stable amino ketone[56]. Dehydration, incorporation of NH_3 from PdxT and loss of inorganic phosphate convert the amino ketone to a chromophoric adduct[54-57]. The chromophoric adduct is then combined with G3P to form PLP.

Cytidine Triphosphate Synthetase

CTP

Cytidine triphosphate (CTP) is a pyrimidine nucleotide and one of the four nucleotide building blocks of RNA. For DNA synthesis, CTP is dephosphorylated to cytidine diphosphate (CDP), which is then reduced by ribonucleotide reductase to deoxy-cytidine diphosphate (dCDP), which is phosphorylated to dCTP. Additionally, CTP is the precursor for phospholipid pathway intermediates such as cytidine

diphosphate diacylglycerol (CDP-DG), CDP-choline and CDP-ethanolamine[58,59]. CDP-DG provides the phosphatidyl moiety for phosphatidylserine, phosphatidylethanolamine, phosphatidylcholine, phosphatidylglycerol, cardiolipin and phosphatidylinositol[60,61]. CDP-choline and CDP-ethanolamine provide the hydrophilic head groups for phosphatidylethanolamine, and phosphatidylcholine (Fig. 1.7)[61].

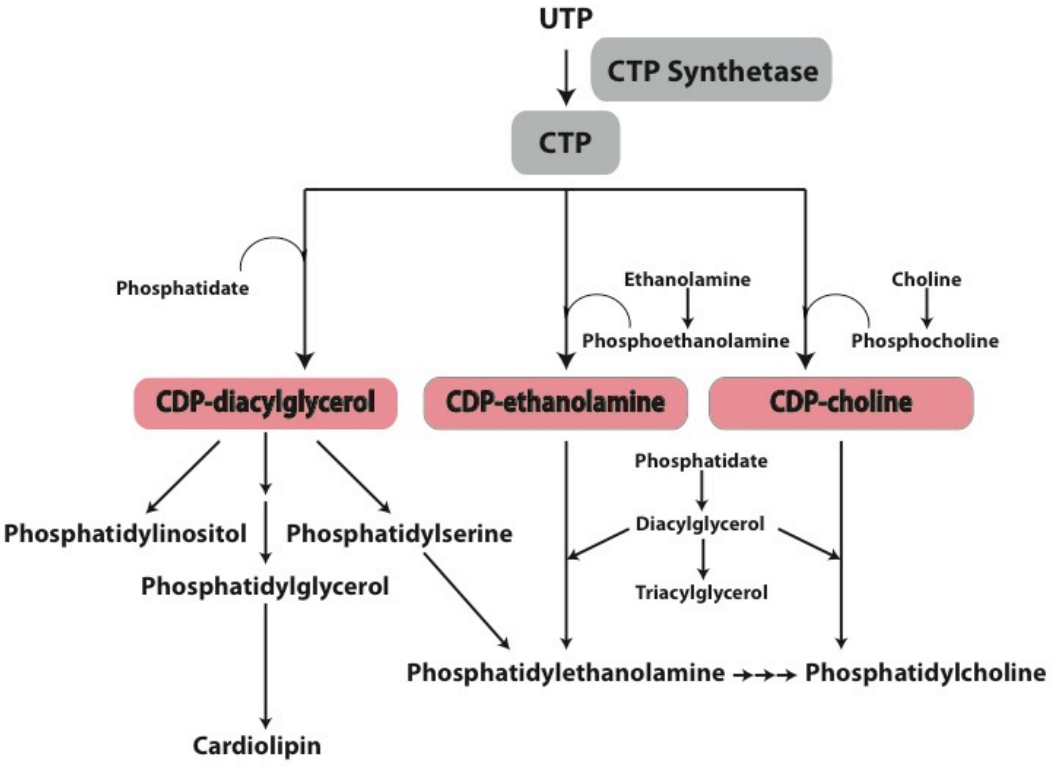

Figure 1.7 The role of CTP synthetase in the synthesis of phospholipids.

RNA, DNA, and phospholipids are essential to cell proliferation. Therefore, understanding the biosynthetic pathway for CTP provides a useful target for cancer treatment. Cancer cells have elevated and unregulated levels of CTP biosynthesis, demonstrating how important and directly correlated CTP biosynthesis is to oncology[62,63]. Cancer cells differ from normal cells in their use of the rapid oxygen-

independent pathway of glycolysis to produce the cell's energy, known as the Warburg effect[64]. Glycolysis generates the building blocks for nucleotides (ribose 5-phosphate) and phospholipids (glycerol), which are necessary for cell replication and tumor maintenance[65].

CTP Biosynthesis

The biosynthesis of CTP through amination of uridine triphosphate (UTP) was first discovered in *Escherichia coli* (Fig. 1.8)[66]. The pathway is dependent on ammonia, adenosine triphosphate (ATP), magnesium and UTP and is the only biosynthetic route to CTP[66]. Further characterization revealed that CTP formation is most efficient with glutamine as the nitrogen source (although ammonia can substitute) and is tightly regulated by other nucleotides: guanosine triphosphate (GTP) is a potent activator and the product, CTP, is a potent inhibitor[67-70]. GTP activation is observed only when glutamine is the nitrogen source[71].

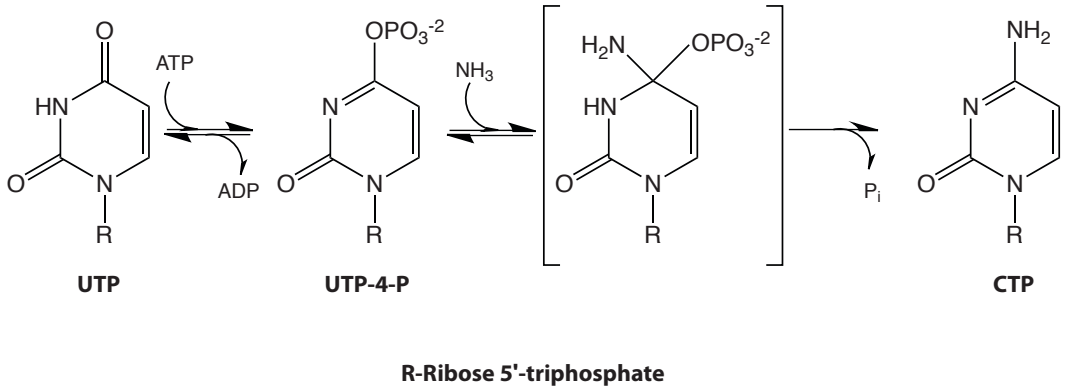

Figure 1.8 CTP biosynthesis

The enzyme responsible for generating CTP, CTP synthetase (CTPS), was purified first from *E. coli* and identified as a homotetramer, with each monomer

containing all the necessary active sites needed to convert UTP to CTP[67,72]. Although the active enzyme complex is a homotetramer, it has been shown that at low CTPS concentrations and in the absence of nucleotide substrates, CTPS will dissociate to a dimer[73-75]. The mechanism of CTPS proceeds through phosphoryl activation of UTP at the O4 position in the presence of ATP and Mg^{+2}, creating the attack site for NH_3, ending in the release of phosphate, CTP and ADP[7,74]. Further investigation revealed that CTPS is a GAT, and forms a glutamyl-thioester intermediate during the reaction mechanism[76]. Glutaminase activity is dependent on the presence of the acceptor substrates (UTP and ATP), as it is for most GATs[74].

Nucleotides not only affect the oligomerization of CTPS, but also its activity. CTPS exhibits positive cooperativity for each of UTP and ATP when the concentration of the other is limiting[67,73]. Under saturating concentrations, binding of UTP and ATP occurs in a Michaelis-Menten manner[67,73]. CTPS glutaminase activity is increased 3-4 fold in the presence of GTP[7,77]. GTP accelerates the glutamylation of CTPS, increasing the k_{cat} and decreasing the K_m of this step, while having no effect on the NH_3-mediated CTP formation[71]. Kinetic studies suggest that GTP increases the affinity for and stabilization of the tetrahedral intermediate of glutamine hydrolysis[78]. The concentration range for GTP activation is very narrow. Concentrations exceeding 0.15 mM GTP inhibit CTP formation while having no effect on glutaminase activity, indicating that the nucleotide may bind competitively to the other nucleotide binding sites[79].

At high concentrations, CTP acts as a competitive inhibitor[67]. CTP was speculated to occupy the same binding site as UTP[67], however, a crystal structure of CTPS co-crystallized with CTP revealed that this was only partially true[77]. The UTP and

CTP triphosphate binding sites overlap, whereas the nucleosides occupy two binding sites that differ by a rotation of ~120° [77,80]. This prevents UTP and CTP binding to CTPS at the same time and prevents wasteful generation of CTP. The intricate role of each nucleotide concentration in regulating CTPS activity ensures that nucleotide concentrations are maintained in proper balance. Deregulation of CTPS abolishes the cell's natural checkpoint allowing the overproduction of CTP, which leads to the overproduction of phospholipids, DNA and RNA, supporting excessive cell proliferation[62,63,81]. In addition to being a target for cancer therapy, CTPS has been shown to play a role in the human immune system. A mutation was identified that resulted in an impaired capacity of activated T and B cells to proliferate in response to antigen receptor–mediated activation[81]. These results suggest that CTPS may also be a target for auto- or allogenic-specific T-cell and B-cell therapies[81].

CTPS

CTPS is conserved across both eukaryotes and prokaryotes. Yeast and mammals have two isoforms of CTPS[82-84]. In mammals these isoforms share 74% identity[84]. The gene for CTPS from *E. coli* encodes 544 amino acids, whereas that from yeast encodes 570 amino acids[82,85]. CTPS is comprised of an N-terminal synthetase domain followed by an interdomain linker and a C-terminal class I Triad glutaminase domain[85,86]. The CTPS tetramer has an overall X shape with D_2 symmetry (Fig. 1.9). The synthetase domains interact, supporting the core of the complex, while the glutaminase domains form arms of the X[86,87].

The glutaminase domain is made up of a core seven-stranded parallel β-sheet, with the exception of β6, which is antiparallel to the rest. On one side of the core β-

sheet are two antiparallel β-strands and five α-helices[86,87]. On the other side there are three β-strands, two parallel and one antiparallel, and five α-helices[86,87]. The conserved catalytic triad includes residues Cys378, His502, and Glu504[85-87]. The backbone amides of Gly349 and Leu377 make up the oxyanion hole[87].

The synthetase domain is composed of a core β-sheet consisting of 7 parallel β-strands, which is sandwiched between helical layers with 5 α-helices on each side[86,87]. ATP binds within a single subunit, and a hydrogen bond to the N6 adenine base creates nucleotide specificity by preventing GTP from binding to this site[77,80]. UTP binds between subunits, with the uracil base contained within the same subunit as ATP, and the triphosphate binding to the adjacent subunit[77]. The triphosphate of CTP binds to the same site as the UTP triphosphate while the sugar-base is rotated around the C4' -C5' bond and positioned in a cleft created by three different subunits[77,80]. The GTP binding site is unknown. Many attempts to elucidate this binding site and determine how GTP binding influences glutaminase activity have been unsuccessful.

Thesis Overview

The focus of this thesis is to elucidate key residues/structural elements that contribute to the multi-step catalysis of two Triad GATs (PLPS from *G. stearothermophilus* and CTPS from *A. aeolicus*). In this study I am interested in investigating the structural changes induced by either binding of the acceptor substrates or binding of an allosteric activator and determining which amino acids propagate the conformational changes that are essential to the mechanism. X-ray crystallography was used to study structures of each protein with covalent intermediates, providing snapshots of the enzyme in its catalytic cycle. Mutagenesis, enzyme kinetics and

biochemical assays were used to investigate specific sites deemed to be critical to a definitive step in each enzyme's mechanism.

To investigate the mechanism and the role of the C-terminal tail of the synthase subunit (PdxS) of PLPS, three crystal structures were obtained with either the synthase subunit alone (PdxS/R5P and PdxS/R5P/NH_3) or the intact protein (PLPS/R5P/Gln). These structures represent the three different known intermediates generated during the catalytic cycle. Each intermediate was trapped using either site directed mutagenesis and/or biochemical assays to optimize the conditions specific to each intermediate. Structural elements that experienced conformational changes were probed by site-directed mutagenesis to identify which residues are important and how they affect mechanism.

To elucidate the GTP binding site on CTPS and identify how binding enhances glutaminase activity, X-ray crystallography, mutagenesis and biochemical assays were used to probe the individual domains and the intact CTPS homotetramer. I obtained a structure of CTPS co-crystallized with a glutamine analog (6-diazo-5-oxo-L-norleucine; DON) to promote the binding of GTP with a Michaelis-Menten complex of CTPS. Biochemical assays were used to probe each domain individually to determine where GTP binds.

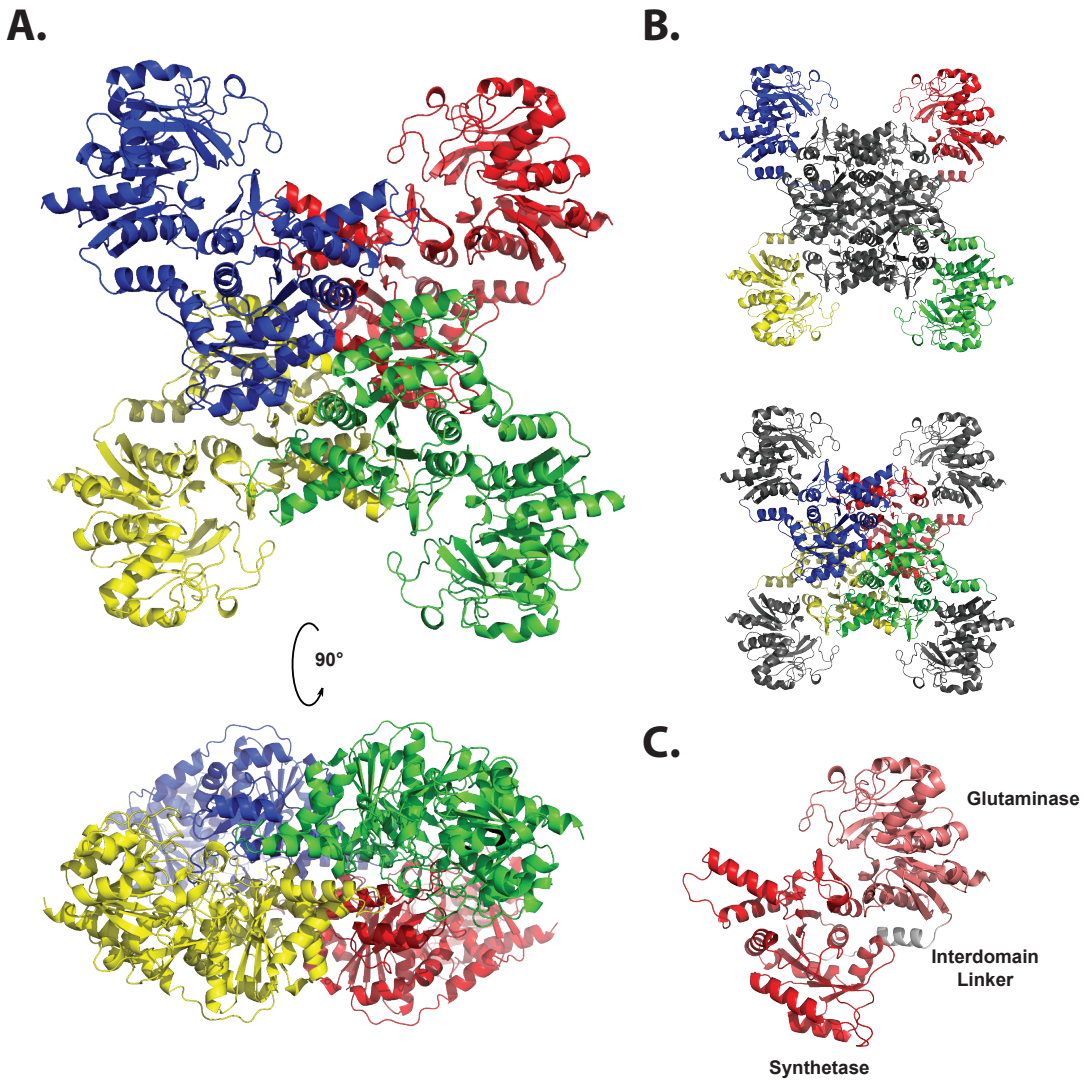

Figure 1.9 Overall architecture of CTPS. A. CTPS homotetramer[77]. The overall shape of CTPS is an X with D_2 symmetry. B. TOP: The glutaminase domains (colored) generate each arm of the overall X shape. BOTTOM: The synthetase domains (colored) interact, supporting the core of the complex. C. Each monomer is comprised of a N-terminal synthetase domain (red) followed by an interdomain linker (gray) and ending with a C-terminal glutaminase domain (pink).

Chapter 2

Structural Investigation into the Mechanism of the Synthase Subunit of PLPS.

Summary

PLP synthase (PLPS) generates the highly utilized co-factor pyridoxal 5'-phosphate (PLP), from common readily available cell metabolites (glutamine, ribose 5-phosphate (R5P) and glyceraldehyde 3-phosphate (G3P)). PLPS is a D_6-symmetric complex of 12 synthase subunits (PdxS) and 12 Triad glutaminase subunits (PdxT). PdxT and PdxS have distinct and remote functions. PdxT functions as a Triad glutaminase using a Cys-His-Glu triad to hydrolyze glutamine to glutamate and ammonia. The ammonia is channeled to the active site of PdxS, which functions as a synthase combining ammonia with G3P and R5P. The mechanism and residues responsible for the combination of ammonia (from PdxT), R5P and G3P has escaped biochemical analysis. Pieces of the catalytic pathway have been confirmed including the identification of two covalent intermediates and substrate binding order. First, R5P and PdxS (Lys81) form a Schiff base that isomerizes to a stable amino ketone, in a manner independent of PdxT, glutamine or G3P[40,56]. Dehydration, incorporation of NH_3 (from PdxT) and loss of inorganic phosphate convert the amino ketone to a chromophoric adduct[54,55,57]. To investigate the mechanism of the synthase subunit, I obtained two crystal structures of synthase complexes (PdxS/R5P and PdxS/R5P/NH_3). The structures provide snapshots of PdxS at distinct steps in its complicated catalytic cycle and provide insights into the

elusive mechanism and structural elements that drive the conversion of amino ketone to chromophore. The structure of PdxS with R5P contains two covalent adducts, pentulose phosphate modifications on Lys81 and Lys149. They differ in attachment to R5P (C1 or C2). The unexpected adduct at Lys149 implies that Lys149 may play a role in either the conversion of the amino ketone to the chromophore or G3P binding. The structure of PdxS with R5P in the presence of NH_3 captures three distinct states in the 12 active sites of the crystallographic asymmetric unit, providing snapshots of PdxS from amino ketone to chromophore formation. Additionally, Lys149 is flipped into the active site, as opposed to its position outside of the active site observed in every other structure of the synthase subunit. Through biochemical assays and a comparison of the two crystal structures, I identified residues important to the conversion of the amino ketone to the chromophore and a second phosphate-binding site residing outside of the R5P active site that appears to play a role in PLP formation post chromophore formation.

Introduction

Pyridoxal 5-phosphate synthase (PLPS) is a single enzyme route for generating PLP in organisms that utilize the deoxyxylulose 5-phosphate (DXP) independent pathway[33]. PLPS is a 24-subunit enzyme comprised of two subunits, $PdxS_{12}$ and $PdxT_{12}$ (Fig. 2.1)[9]. PdxT functions as a Triad glutaminase domain, using the catalytic triad Cys-His-Glu to hydrolyze glutamine to glutamate and ammonia (Fig. 2.2)[8]. Ammonia produced in PdxT is channeled to the active site of PdxS where it participates in the second reaction of the bi-catalytic enzyme (Fig

2.3)[40]. PdxS functions as a remarkable synthase using simple readily available precursors from PdxT (NH_3), glycolysis (G3P) and the pentose phosphate pathway (R5P) as substrates[8,40]. Dissecting the mechanism of the synthase subunit of PLPS has proven to be challenging. Biochemical analysis has revealed pieces of the mechanism but trying to put the pieces together has been difficult. Order of substrate binding and identification of covalent intermediates has been imperative to elucidating the step-by-step catalytic mechanism of PdxS.

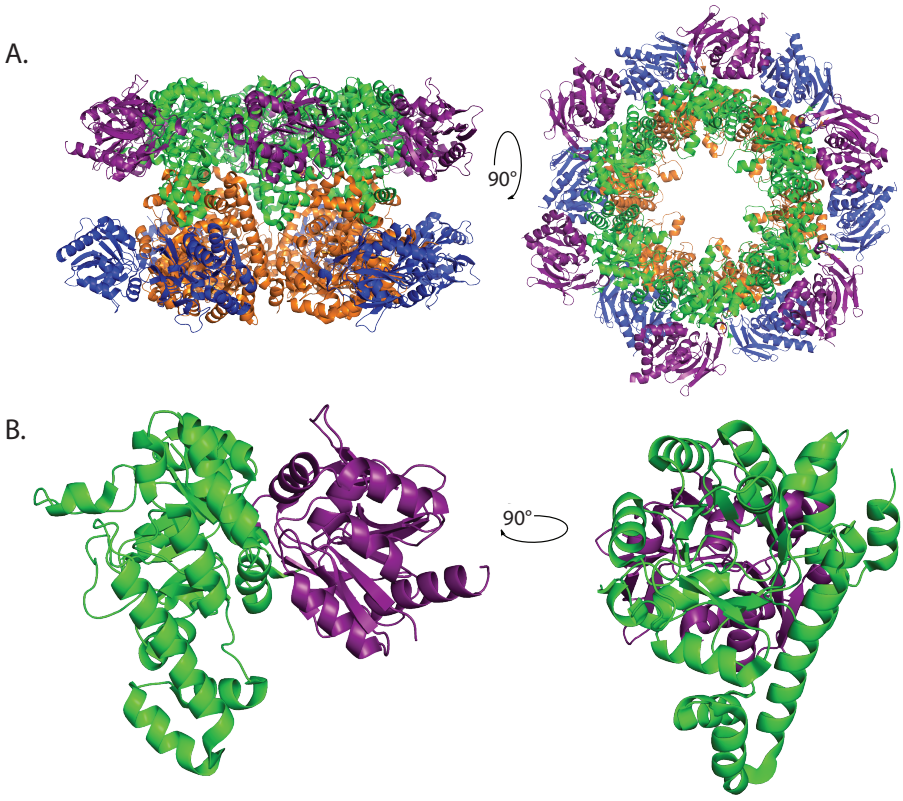

Figure 2.1 Structure of PLPS. A. PLPS (PDB: 2NV2) is a 24-mer made up of $PdxS_{12}$ (orange and green) and $PdxT_{12}$ (purple and blue). B. The catalytic protomer consists of one monomer of PdxS (green) and one monomer of PdxT (purple)[9].

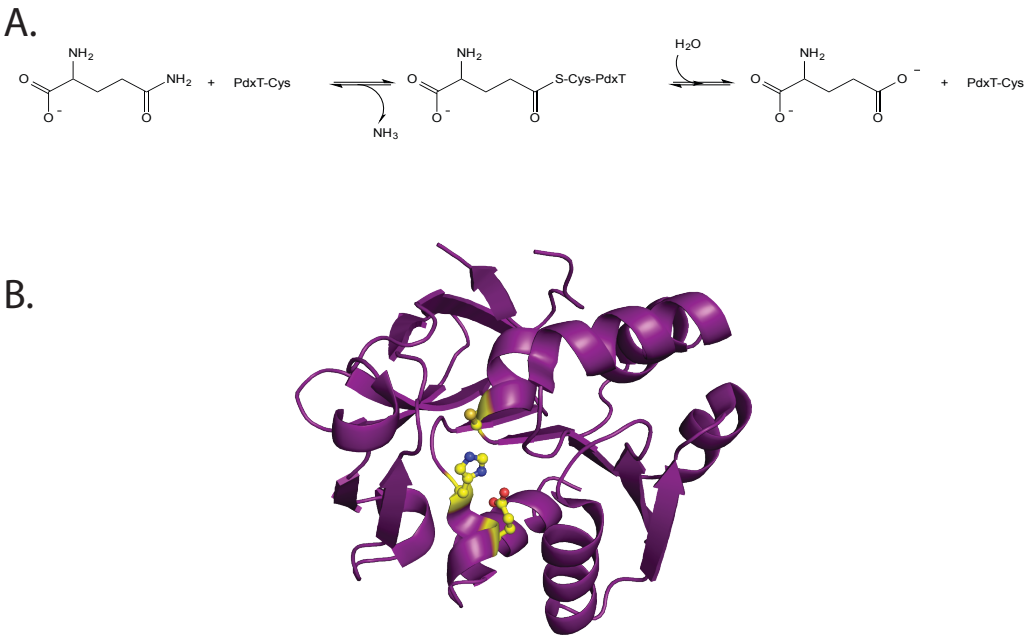

Figure 2.2 PdxT functions as a glutaminase. A. PdxT hydrolyzes glutamine to generate glutamate and ammonia. B. PdxT (PDB: 2ISS, *T. maritima; purple)* uses a catalytic triad (His, Glu, Cys; yellow sticks) to hydrolyze glutamine[49].

PdxS binds one substrate at a time, building on an initial Schiff base intermediate between R5P and an active site lysine that isomerizes to form an amino ketone (Fig. 2.3)[40,56]. The presence of the amino ketone has been confirmed through mass spectrometry (MS) and nuclear magnetic resonance (NMR)[40,55,56]. The formation of the covalent intermediate is not dependent on the presence of PdxT, glutamine or G3P[40]. The intermediate has been observed in a crystal structure of PLPS from *Thermotoga maritima*[40,49,55,56]. Two different groups have confirmed the mass of the intermediate to be 212 Da,[40,55] corresponding to the addition of R5P (230 Da) and loss of a water molecule (-18 Da). Initial experiments (trypsin digest followed by MS-MS) identified the invariant Lys149 as the site of the intermediate[55]. The role of Lys149 and the identification of the R5P carbon

attached to the lysine have been controversial. In contrast to the MS-MS results, the PLPS structure from *T. maritima* revealed that the lysine modified was Lys81 and not Lys149[49].

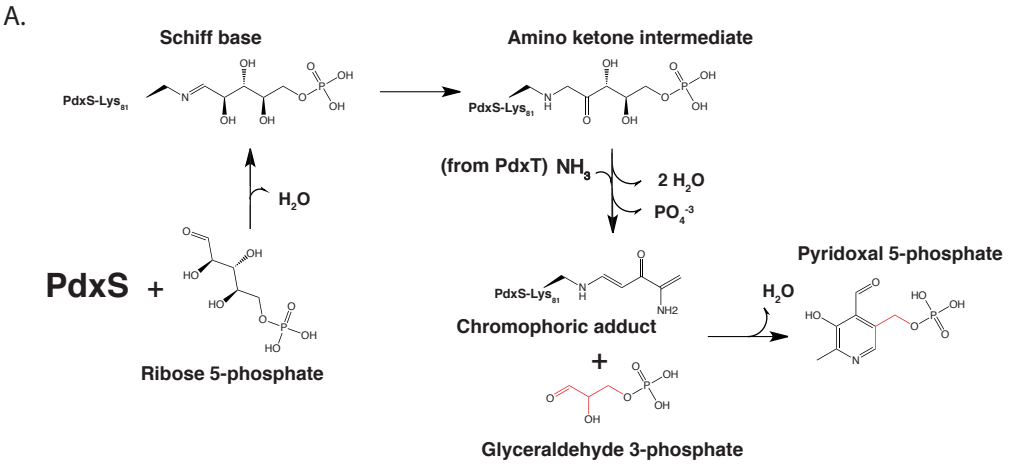

B.

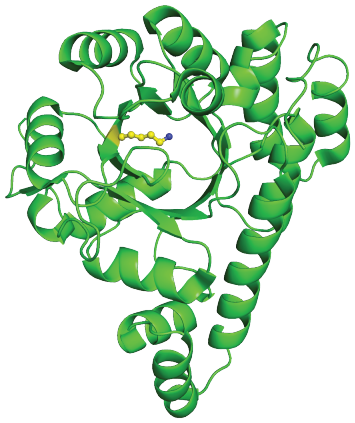

Figure 2.3 PdxS functions as a synthase. A. The mechanism of PdxS proceeds through two covalent intermediates[40,55]. B. Lys81 (yellow spheres) is the site of covalent attachment[49]. (PDB: 2ISS, *T. maritima,* green).

Based on the occupancy and the steric constraints for the phosphate group of the pentulose phosphate adduct, the covalent adduct in the PLPS structure from *T. maritima* was modeled as a C2 attachment (Fig. 2.4)[49]. Although the enzyme

was co-crystallized with R5P, R5P and ribulose 5-phosphate (5RP) readily interconvert, allowing the pentose phosphate sugar to form a Schiff base either through C1 (a highly reactive aldehyde on R5P) or C2 (a ketone on 5RP) supporting the possibility for either attachment. The structure with the Lys81 adduct led to the hypothesis of a hand-off between Lys81 and Lys149 on the reaction pathway[49]. Kinetic experiments revealed a preference for R5P over 5RP, based on K_m values, suggesting that a C1 attachment is preferred[55]. NMR experiments revealed that the lysine adduct is attached through C1[56].

Figure 2.4 The first covalent intermediate modeled as a C2 attachment in YaaD from *T. maritima*[49].

Based on these results, a Schiff base at Lys149 appears to be improbable. Nevertheless, the structure of the synthase subunit alone (Snz) from

Saccharomyces cerevisiae co-crystallized with PLP shows PLP bound outside of the synthase active site and forming a hydrogen bond with Lys149[50]. Once again the hypothesis of a Lys81 hand-off to Lys149 resurfaced, supporting the idea that in the process of product generation, the first covalent intermediate occurs at Lys81 (inside the active site), somewhere along the catalytic pathway it is combined with G3P, and the product associates with Lys149 outside of the active site. However, in all reported structures of the synthase subunit or the intact PLPS enzyme, Lys149 is always pointed outside of the active site[9,48-50].

The next piece of the catalytic puzzle was the identification of a second covalent adduct. In the presence of ammonia (more effectively when glutamine is the nitrogen source), the amino ketone isomer is converted to a chromophoric covalent intermediate with a wavelength maximum at 315 nm[55]. MS experiments revealed that the mass of this new adduct is 95 Da[55]. This corresponds to the loss of two water molecules, inorganic phosphate and the incorporation of NH_3[54]. Isotope experiments revealed that the release of phosphate is through a beta elimination resulting in a double bond between C4 and C5[54]. NMR experiments identified C2 as the site of ammonia incorporation and analyzed the structure of the chromophore[56,57].

The combination of G3P with the chromophore to form PLP is the remaining catalytic step. The binding site of G3P is still unknown. It is also unknown whether G3P incorporation is dependent on any catalytic residues or based solely on proximity and correct orientation to the chromophore. The structure of the synthase subunit alone (Snz) from *S. cerevisiae* co-crystallized with a large excess of G3P

shows G3P binding outside of the active site between adjacent subunits. This site contradicts the conventional substrate binding inside the barrel for all proteins with the β_8/α_8 fold.

The objective was to crystallize the synthase subunit (PdxS) with each covalent adduct in order to elucidate the global conformation changes associated with each intermediate. In order to stabilize each covalent intermediate, specific conditions were optimized. The resulting structures permit a greater understanding of the synthase mechanism and how all the pieces fit together, including identifying residues that participate in the conversion of the amino ketone to the chromophore, affirmation of the carbon attachment of R5P and a view of the structure of the chromophore. Additionally, I have gained insights into potential binding sites for G3P, leading to a more comprehensive mechanistic proposal.

Experimental Procedures

Cloning of G. stearothermophilus *pdxS* -

The plasmid pET0881[48] for PdxS was used for all mutagenesis and sub-cloning. Some substitutions in PdxS (D24N, D24A, D102A, R147K, R147A, and R147Q) were generated by site directed mutagenesis (SDM) (QuikChange by Strategene). SDM primers are listed in table 2.1. PdxS K149 substitutions were generated by SDM (Table 2.1) followed by sub-cloning and insertion into an appropriate expression vector (K149R and K149Q cloned into pTrc-9, K149A cloned into pMCSG9). Primers used to sub-clone *pdxS* out of pET0881 are listed in Table 2.2. The remaining substitutions were generated by SDM on the wild type *pdxS* gene that had been sub-cloned into an appropriate expression vector Table 2.1. Dr. Clay

Brown constructed the pTrc-9 vector from pMCSG9 by cleaving pMCSG9 with restriction endonucleases Sph I and Nde I. This removes the T7 promoter, *lac* operator and ribosome binding site sequences. These sequences were replaced by insertion of a synthetic DNA carrying the *trp/lac* fusion promoter *trc*[88], the translational enhancer sequence for the *E. coli atp* genes[89] and the ribosome binding site (AGGAGG) spaced eight base-pairs from the ATG start sequence[90]. All mutagenesis was verified by sequencing.

Table 2:1 Primers used for SDM.

Plasmid Name	Mutation	Expression Vector	Direction	Primer
pET0881_D24N	PdxS D24N	pET0881	Forward	5'-GCGGCGTCATCATGAACGTCGTGAACGCA-3'
pET0881_D24A	PdxS D24A	pET0881	Forward	5'-CGGCGTCATCATGGCCGTCGTGAACGCAG-3'
pET0881_D102A	PdxS D102A	pET0881	Forward	5'-CTTGGTGTCGACTACATTGCCGAAAGTGAAGTATTAACG-3'
pET0881_R147K	PdxS R147K	pET0881	Forward	5'-AAGGGGCATCGATGTTGAAAACCAAAGGAGAGCCGG-3'
pET0881_R147Q	PdxS R147Q	pET0881	Forward	5'-GGGCATCGATGTTGCAAACCAAAGGAGAGCC-3'
pET0881_R147A	PdxS R147A	pET0881	Forward	5'-GGGGCATCGATGTTGGCAACCAAAGGAGAGCC-3'
pPdxSMBP_K149R	PdxS K149R	pET0881	Forward	5'-CGGCTCTCCTCTGGTTCGCAACATCGATGC-3'
pPdxSMBP_K149Q	PdxS K149Q	pET0881	Forward	5'-CGATGTTGCGAACCCAGGGAGAGCCGGGGAC-3'
pPdxSMBP_K149A	PdxS K149A	pET0881	Forward	5'-TCGATGTTGCGAACCGCAGGAGAGCCGGGGAC-3'
pPdxS_E103Q	PdxS E103Q	pMCSG7	Forward	5'-CCGGCGTTAATACTTCACTCTGGTCAATGTAGTCGACACCA-3'
pPdxS_E103A	PdxS E103A	pMCSG7	Forward	5'-GTGTCGACTACATTGACGCAAGTGAAGTATTAACGCC-3'
pPdxSMBP_H115Q	PdxS H115Q	pMCSG9	Forward	5'-GGCTGATGAGGAATTCCAGATTGACAAACGGCAGTTT-3'
pPdxS_H115A	PdxS H115A	pMCSG7	Forward	5'-GCCGGCTGATGAGGAATTCGCTATTGACAAACGGCAGTTT-3'
pPdxSMBP_R130Q	PdxS R130Q	pMCSG9	Forward	5'-TTTGTGTGCGGTTGCCAGGATTTAGGGGAAGCGG-3'
pPdxSMBP_R130A	PdxS R130A	pMCSG9	Forward	5'-CGCTTCCCCTAAATCGGCGCAACCGCACACAAAT-3'
pPdxS_R137Q	PdxS R137Q	pMCSG7	Forward	5'-GGGGAAGCGGCGCAGCGCATTGCAGAAG-3'
pPdxS_R137A	PdxS R137A	pMCSG7	Forward	5'-TTCTGCAATGCGGGCCGCCGCTTCCCCT-3'
pPdxSMBP_R138K	PdxS R138K	pMCSG9	Forward	5'-TGCCCCTTCTGCAATCTTGCGCGCCGCTTCCCC-3'
pPdxSMBP_R138E	PdxS R138E	pMCSG9	Forward	5'-GGGAAGCGGCGCGCGAGATTGCAGAAGGGGC-3'
pPdxSMBP_R138Q	PdxS R138Q	pMCSG9	Forward	5'-GAAGCGGCGCGCCAGATTGCAGAAGGGG-3'
pPdxSMBP_R138A	PdxS R138A	pMCSG9	Forward	5'-GGAAGCGGCGCGCGCCATTGCAGAAGGG-3'
pPdxSMBP_R137QR138Q	PdxS R137QR137Q	pMCSG9	Forward	5'-TTTAGGGGAAGCGGCGCAGCAGATTGCAGAAGGGGCATC-3'
pPdxSMBP_R137AR138A	PdxS R137AR138A	pMCSG9	Forward	5'-GCCCCTTCTGCAATGGCGGCCGCCGCTTCCCCTAA-3'
pPdxSMBP_K187Q	PdxS K187Q	pMCSG9	Forward	5'-GAGCCCCGAGCTGCTGCGCCTCAGCGACA-3'
pPdxSMBP_K187A	PdxS K187A	pMCSG9	Forward	5'-GAGCCCCGAGCTGTGCCGCCTCAGCGACAA-3'

Table 2:2 Primers used to sub-clone *pdxS.*

Primer Name	Template	Direction	Primer	Expression Vectors
PdxS Start 3	pET0881	Forward	5'-TACTTCCAATCCAATGCAAGCACAGGTACGGAC-3'	pMCSG7, pMCSG9, pTrc-9
PdxS Stop LIC	pET0881	Reverse	5'-TTATCCACTTCCAATGTTACCAGCCGCGTTCTTG-3'	pMCSG7, pMCSG9, pTrc-9

Expression and Purification of PdxS and PdxT:

PdxS and PdxT were purified separately. Cells of *E. coli* strain BL21(DE3) (or strain BL21 for pPdxSMBP_K149R and pPdxSMBP_K149Q) were transformed with the appropriate expression plasmid, grown at 37°C in either Luria-Bertani (LB)

or Terrific Broth (TB) medium until OD_{600} reached 0.8 for LB and 1 for TB. The temperature was reduced to 20°C for 1 hr, expression was induced with either 200 μM (TB) or 400 μM (LB) IPTG, and cultures were incubated 12-16 hr (specifics listed in Table 2.3). All purification steps were carried out at 4°C unless otherwise noted. Cells from a 1 L culture were harvested by centrifugation, re-suspended in 40 mL of Buffer A (20 mM Tris-HCl pH 7.9, 500 mM NaCl), lysed by sonication, and centrifuged at 18,000 x g. The supernatant was filtered and loaded onto a Ni^{+2} affinity column (HisTrap™ HP, GE Healthcare). Bound protein was eluted with a linear gradient of 0-500 mM imidazole in Buffer A. The N-terminal His_6-tag of PdxS was removed by TEV protease by 4 hr digestion at room temperature followed by dialysis (Buffer A). TEV protease and un-cleaved PdxS were removed by Ni^{+2} affinity chromatography. Proteins intended for crystallization were further purified by gel filtration. PdxS was purified on an S300 column (HiPrep™ 16/60 Sephacryl™ S-300 HR, GE Healthcare) using 20 mM Tris-HCl pH 8.5, 500 mM NaCl, 10 mM glutamine, 2 mM DTT. PdxT was purified on an S100 column (HiPrep™ 16/60 Sephacryl™ S-100 HR, GE Healthcare) using 20 mM Tris-HCl pH 7.9, 500 mM NaCl, 2 mM DTT. Individual subunits were concentrated and stored at -80°C.

Table 2:3 Specific growth conditions for each construct.

Plasmid	Mutation	Expression Vector	Media	Antibiotic	[IPTG] μM
pET0881_D24N	PdxS D24N	pET0881	LB	Kan	400
pET0881_D24A	PdxS D24A	pET0881	LB	Kan	400
pET0881_D102A	PdxS D102A	pET0881	LB	Kan	400
pET0881_R147K	PdxS R147K	pET0881	LB	Kan	400
pET0881_R147Q	PdxS R147Q	pET0881	LB	Kan	400
pET0881_R147A	PdxS R147A	pET0881	LB	Kan	400
pPdxSMBP_K149R	PdxS K149R	pTRC9	TB	Amp	200
pPdxSMBP_K149Q	PdxS K149Q	pTRC9	TB	Amp	200
pPdxSMBP_K149A	PdxS K149A	pMCSG9	TB	Amp	200
pPdxS_E103Q	PdxS E103Q	pMCSG7	TB	Amp	200
pPdxS_E103A	PdxS E103A	pMCSG7	TB	Amp	200
pPdxSMBP_H115Q	PdxS H115Q	pMCSG9	TB	Amp	200
pPdxS_H115A	PdxS H115A	pMCSG7	TB	Amp	200
pPdxSMBP_R130Q	PdxS R130Q	pMCSG9	TB	Amp	200
pPdxSMBP_R130A	PdxS R130A	pMCSG9	TB	Amp	200
pPdxS_R137Q	PdxS R137Q	pMCSG7	TB	Amp	200
pPdxS_R137A	PdxS R137A	pMCSG7	TB	Amp	200
pPdxSMBP_R138K	PdxS R138K	pMCSG9	TB	Amp	200
pPdxSMBP_R138E	PdxS R138E	pMCSG9	TB	Amp	200
pPdxSMBP_R138Q	PdxS R138Q	pMCSG9	TB	Amp	200
pPdxSMBP_R138A	PdxS R138A	pMCSG9	TB	Amp	200
pPdxSMBP_R137QR137Q	PdxS R137QR137Q	pMCSG9	TB	Amp	200
pPdxSMBP_R137AR137A	PdxS R137AR138A	pMCSG9	TB	Amp	200
pPdxSMBP_K187Q	PdxS K187Q	pMCSG9	TB	Amp	200
pPdxSMBP_K187A	PdxS K187A	pMCSG9	TB	Amp	200

PLPS Activity Assays:

Formation of the chromophoric adduct of R5P and NH_3 with PdxS was assayed at 37°C in a total reaction volume of 50 μL containing 50 μM PdxS, 50 μM PdxT, 50 mM Tris-HCl pH 7.9, 20 mM glutamine and 10mM R5P[55]. The chromophoric adduct was detected by absorbance at 315 nm in a SpectraMax M5.

PLP synthesis was assayed at 37°C in a total reaction volume of 50 μL containing 50 μM PdxS, 50 μM PdxT, 50 mM Tris-HCl pH 7.9, 20 mM glutamine, 10mM R5P, 20 mM G3P. PLP was detected by absorbance at 415 nm in a SpectraMax M5.

Chromophore formation and PLP synthesis for PdxS mutants at Lys149 were assayed in a sub-micro quartz cuvette (Starna Cells, Inc.) with a total reaction volume of a 100 μL using an Ultrospec 3100 pro spectrophotometer (Amersham Biosciences).

Intact Protein Mass Spectrometry

For detection of covalent adducts of PdxS, reaction mixtures of total volume 100 µL were incubated 15 min at 37°C, quenched with 10% formic acid and analyzed by LC-MS. Samples were eluted at a flow rate of 0.5 mL/min, with a linear gradient of 5% to 95% acetonitrile, over 15 min employing a Aeris widepore C4 column (3.6 µm, 50 x 2.10 mm) and directly analyzed by ESI mass spectrometry (Agilent 6520 Accurate Mass Q-TOF). Data were analyzed using the maximum entropy deconvolution algorithm within the Agilent Mass Hunter Qualitative Analysis software.

Assays of covalent adduct formation at Lys81 in PdxS D24N, D24A, R147K, R147Q and R147A were carried out with 150 µM PdxS and 200 µM PdxT, 20 mM Tris-HCl pH 7.9, 10 mM R5P, 20 mM Gln. Assays of adduct formation in wild type PLPS were carried out with 31.25 µM PdxS, 60 µM PdxT, 20 mM Tris-HCl pH 7.9, 10 mM R5P, 0-20 mM Gln. Assays of adduct formation in PdxS with various pHs were carried out with 31.25 µM PdxS, 10 mM R5P, 50 mM $(NH_4)_2SO_4$, 20 mM Tris-HCl pH 7.0-8.5. Assays of adduct formation in PdxS with increasing amounts of $(NH_4)_2SO_4$ were carried out with 31.25 µM PdxS, 10 mM R5P, 0-250 mM $(NH_4)_2SO_4$, 20 mM Tris-HCl pH 7.0. Excess substrates were removed using a gel filtration column (PD-10 Desalting column, GE Healthcare), and the eluate was diluted to 1 mg/mL total protein prior to formic acid treatment. Assays of second adduct formation in PdxS were carried out with 31.25 µM PdxS, 25 mM R5P, 20 mM Tris-HCl pH 7.0. Acid-quenched samples were incubated overnight before MS analysis.

Crystallization:

PdxS/R5P was crystallized at 20°C via sitting drop vapor diffusion using 4 µL protein solution (5 mg/mL PdxS, 20 mM Tris-HCl pH 8.5, 25 mM R5P, 20 mM $MgCl_2$) and 4 µL reservoir solution (6% PEG 8K, 200 mM Li citrate, 100 mM Na cacodylate pH 7.0). Crystals appeared within 3 days, grew over 7 days, and were cryo-protected with 15% ethylene glycol in reservoir solution and flash-cooled in liquid nitrogen.

PdxS/R5P/NH_3 was crystallized at 20°C via sitting drop vapor diffusion using 4 µL protein solution (5 mg/mL PdxS, 20 mM Tris-HCl pH 8.5, 25 mM R5P, 20 mM $MgCl_2$) and 4 µL reservoir solution (5.6% PEG 8K, 200 mM ammonium citrate, 100 mM Na cacodylate pH 7.0). Crystals appeared within 3 days and grew over 7 days. Eight hours prior to harvesting, 0.8 µL of 250 mM R5P stock was added to the drop. Crystals were cryo-protected with 15% ethylene glycol in reservoir solution and flash-cooled in liquid nitrogen.

X-ray Data Collection and Processing:

Data were collected at the Advanced Photon Source (APS) on the GM/CA beam line 23ID-D. Data were processed and scaled with the HKL2000 suite (Table 2.4/2.5)[91]. Initial phases for each structure were determined by molecular replacement (MR). PdxS from the PLPS/H169N_T/R5P/Gln structure (Chapter 3) was used to solve the PdxS/R5P structure using the program phaser[92,93]. The PdxS/R5P structure was then used to solve PdxS/R5P/NH_3 also using phaser[93]. Iterative model building was done in COOT[94] and refinement was carried out with

REFMAC[95]. Translation/libration/screw (TLS) groups for both structures were determined using the webserver TLS MD[96,97]. Link records for the PdxS covalent adducts Lys81-R5P, Lys149-R5P and Lys81-chromophore were created using J Ligand[98] while the restraints and coordinates were created using prodrg[99] and the grade server[100]. The final models were validated with MolProbity[101]. The refinement statistics of the final models are summarized in Table 2.5 and Ramachandran plots are shown in Fig. 2.5 and 2.6.

Table 2:4 Scaling statistics for PdxS/R5P and PdxS/R5P/NH_3.

PdxS/R5P						
Shell Limit (Å)		Average I	Average Error	Chi^2	Linear R-factor	Multiplicity
Lower	Upper					
50.00	5.81	199	5.5	1.195	0.058	11.0
5.81	4.62	97.2	2.8	1.448	0.081	11.4
4.62	4.03	97.1	2.9	1.809	0.102	11.4
4.03	3.66	67.2	2.5	1.560	0.122	11.4
3.66	3.40	44.8	2.2	1.473	0.162	11.4
3.40	3.20	28.8	1.9	1.403	0.222	11.5
3.20	3.04	17.6	1.8	1.363	0.333	11.5
3.04	2.91	11.7	1.7	1.303	0.474	11.5
2.91	2.80	8.6	1.7	1.250	0.642	11.4
2.80	2.70	6.8	1.8	1.268	0.838	11.4
All Reflections		**58.6**	**2.5**	**1.408**	**0.129**	**11.4**
PdxS/R5P/NH_3						
Shell Limit (Å)		Average I	Average Error	Chi^2	Linear R-factor	Multiplicity
Lower	Upper					
50.00	4.95	362.3	16.2	1.052	0.053	3.8
4.95	3.93	290.2	13.4	1.464	0.067	3.8
3.93	3.44	159.5	8.3	1.518	0.081	3.8
3.44	3.12	84	5.5	1.263	0.096	3.8
3.12	2.90	42.4	4.1	1.317	0.152	3.8
2.90	2.73	26.6	3.7	1.317	0.219	3.8
2.73	2.59	18.7	3.6	1.246	0.296	3.8
2.59	2.48	13	3.5	1.217	0.417	3.8
2.48	2.38	9.9	3.6	1.195	0.556	3.8
2.38	2.30	7.5	3.7	1.185	0.740	3.8
All Reflections		**102.2**	**6.6**	**1.278**	**0.093**	**3.8**

Table 2:5 Crystallographic data and refinement statistics for PdxS/R5P and PdxS/R5P/NH_3.

	Synthase/R5P	Synthase/R5P/NH_3
Diffraction data		
X-ray Source	APS 23ID-D	APS 23ID-D
wavelength	1.033	1.033
space group	$P3_121$	$P2_1$
unit cell parameters (Å)	179.79, 179.79, 104.57	94.68, 107.20, 178.22
α, β, γ (°)	90, 90, 120	90, 92.24, 90
asymmetric unit	6 PdxS	12 PdxS
resolution limit (Å)	2.70(2.77-2.70)	2.29 (2.35-2.29)
unique reflections	53746	158924
avg. I/σ_I	23.4(3.8)	15.5(2.0)
avg. multiplicity	11.4(11.4)	3.8(3.8)
completeness (%)	100(100)	100(100)
R_{sym}	0.129(0.838)	0.093(0.74)
Refinement		
data range	43.44-2.70	47.35-2.29
Reflections	50930	150841
R/R_{free} (%)	21.8/26.2	19.4/22.5
RMS deviations		
bonds lengths (Å)	0.0112	0.0072
bond angles (deg)	1.4169	1.1374
average B factors ($Å^2$)		
protein	63.2	49.1
water	46.2	48.4
ligands	77.3	67.6
Ramachandran		
Favored (%)	97.4	97.5
Allowed(%)	2.5	2.3
Outlier (%)	0.1	0.2
Number of Atoms		
Protein	10971	22333
Water	193	1015
Ligands	264	154

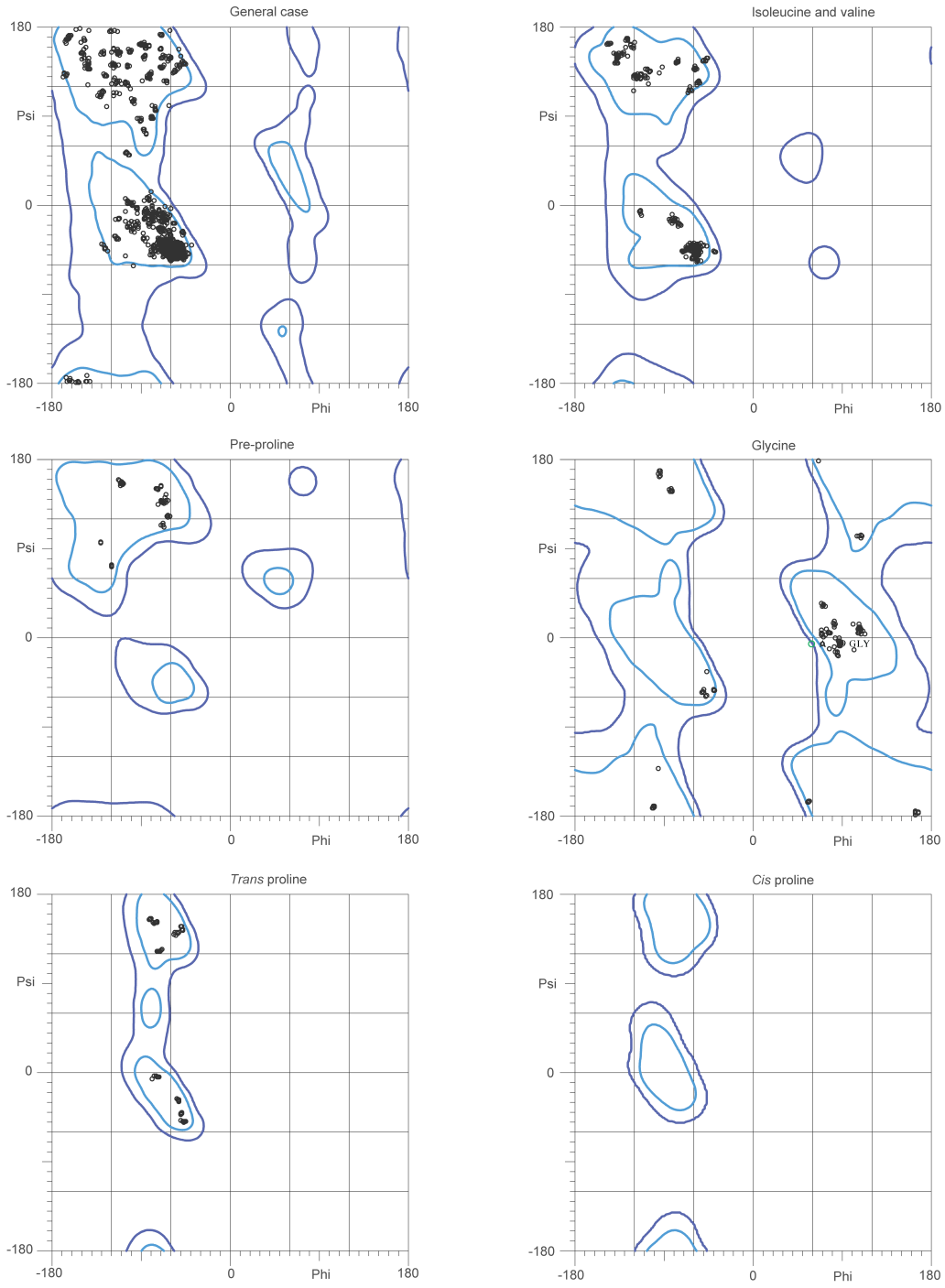

Figure 2.5 Ramachandran plot for PdxS/R5P. Ramachandran plots for PdxS/R5P indicate that 97.4% of all residues were in favored regions and 99.9% of all residues were in allowed regions. Plots were generated using Molprobity[101].

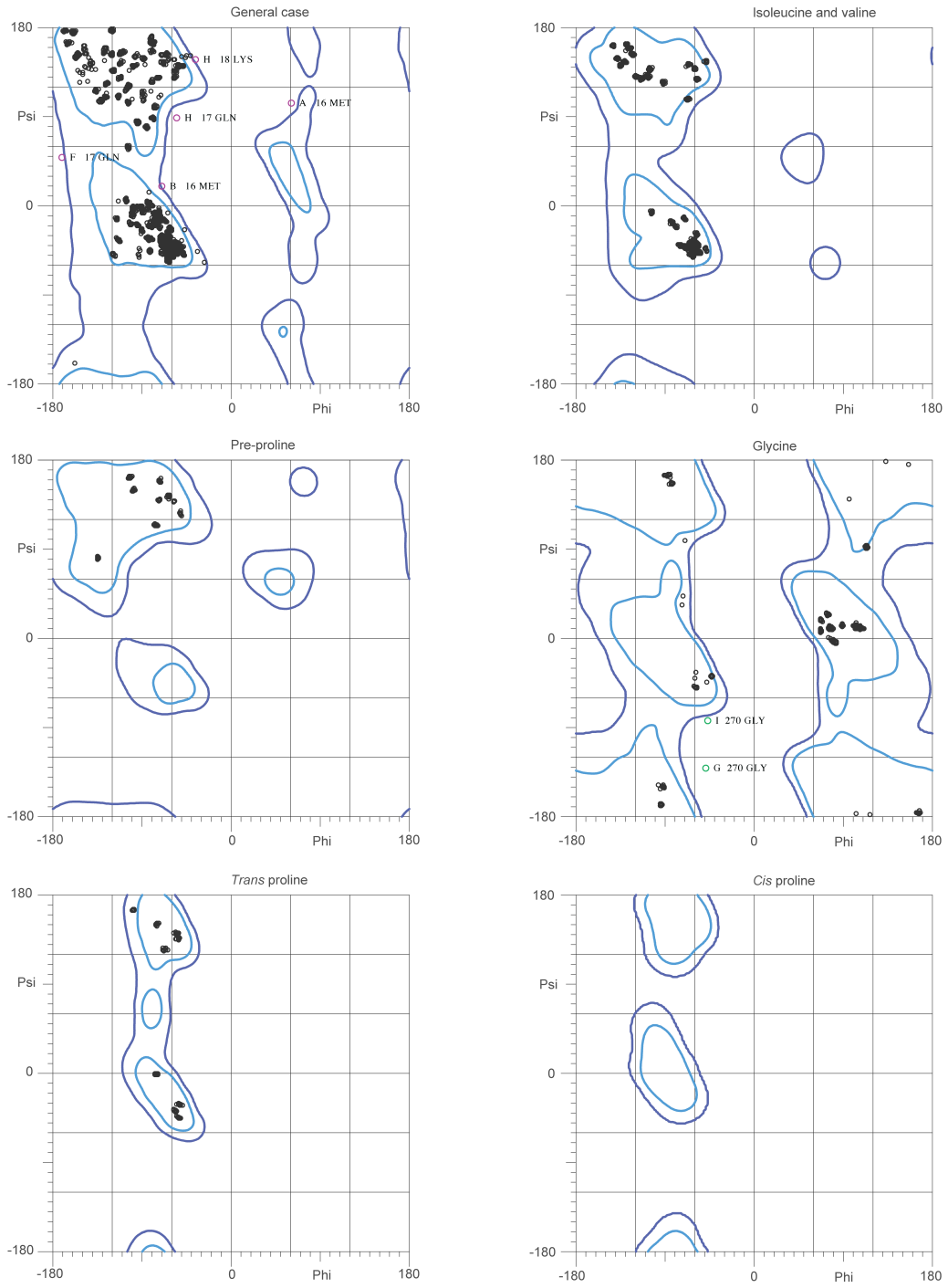

Figure 2.6 Ramachandran plot for PdxS/R5P/NH_3. Ramachandran plots for PdxS/R5P/NH_3 indicate that 97.5% of all residues were in favored regions and 99.8% of all residues were in allowed regions. Plots were generated using Molprobity[101].

Results

First Covalent Intermediate: PdxS Forms a Pentulose Phosphate Adduct with R5P.

I visualized the synthase active site with its first covalent intermediate at Lys81 by co-crystallization of PdxS with R5P (Fig. 2.7). Covalent modification of PdxS in solution was confirmed by whole-protein mass spectrometry (MS) (Fig. 2.8A). The overall dodecameric structure is virtually identical to the structure of the free enzyme form of PdxS[48]. Electron density corresponding to an R5P adduct at Lys81 was present in the active sites of all six subunits in the crystallographic asymmetric unit (Fig. 2.9A). The Lys81 connection had clear density in five active sites and was ambiguous in the sixth. The density is most consistent with formation of a Lys81 adduct at the R5P C1 atom, based on the appearance of unbiased density and the distance between the lysine amino nitrogen and the R5P phosphate. This differs from the C2 Schiff base adduct reported for the *T. maritima* PLPS[49], but is consistent with biochemical data[56]. I modeled and refined the R5P adduct both as the 1-imino, 2-hydroxyl isomer and as the 1-amino, 2-keto isomer. The amino-keto isomer had a better fit to density, as expected[56]. Lys81 is at the top of strand $\beta 3$ in the PdxS β_8/α_8 barrel. The side chain and R5P adduct extends ~15 Å across the barrel with the phosphate near the N-terminus of helix $\alpha 8'$. Despite formation of the adduct, the active site is open perhaps due to the disorder of residues 49-56, which were also disordered in the free enzyme structure[48]. Other contacts of PdxS with the adduct include hydrogen bonds to phosphate oxygens from the amide nitrogens of Gly153, Gly214 and Gly235. Conserved

Asp24 is adjacent to the C2 of the intermediate in position to participate in the formation and isomerization of the Schiff base to the amino ketone. I tested this idea with Ala and Asn substitutions (Table 2.6). The covalent adduct did not accumulate in either of these variants (Fig. 2.10), which also had 100-fold reduced chromophore and PLP formation (Table 2.6). Published results also implicated Asp24 in PLP synthesis[9].

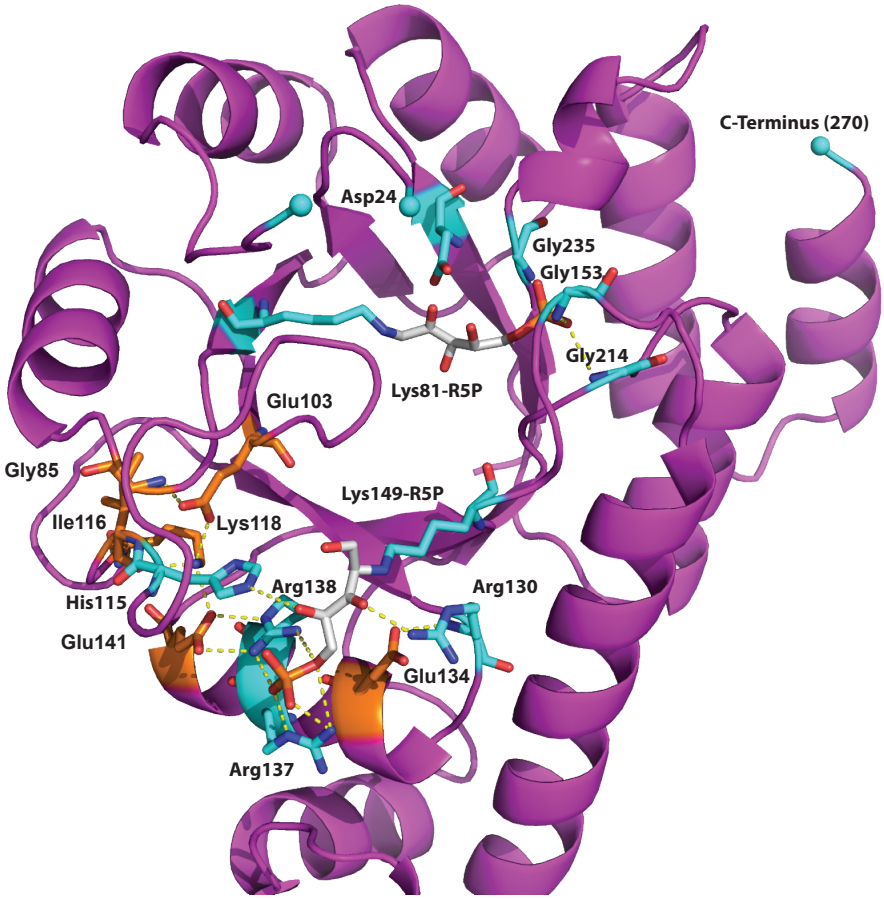

Figure 2.7 Capturing the First Covalent Intermediate: PdxS modified with pentulose phosphate amino ketone. R5P forms a covalent adduct with Lys 81 and Lys149 (PdxS; magenta, R5P; gray sticks, Lys81/Lys149; cyan sticks). Salt bridge network (orange/yellow dashes) surrounding the Lys149 5RP adduct (gray sticks). Residues that interact directly with each covalent adduct are shown in cyan sticks (hydrogen bonds in yellow dashes).

A.

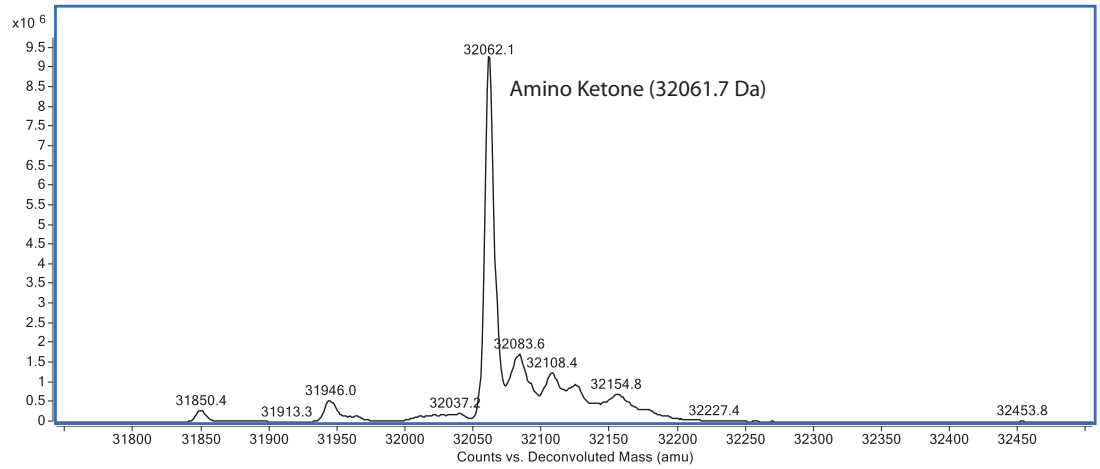

B.

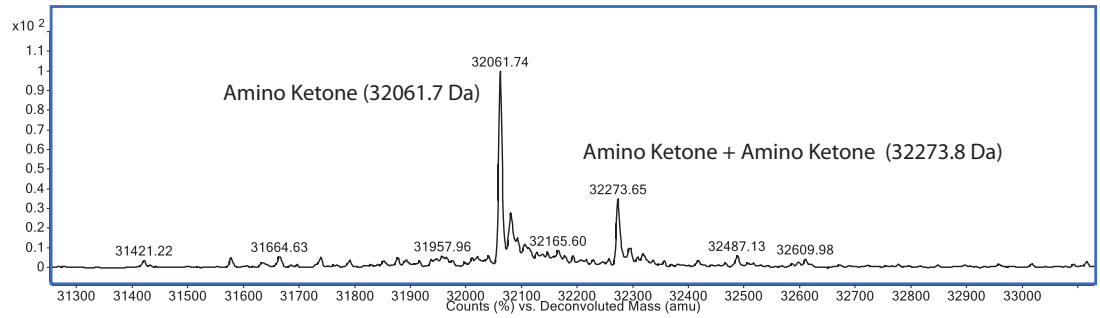

Figure 2.8 Doubly modified PdxS. A. Deconvoluted ESI-mass spectra of PdxS incubated 15 minutes with R5P yields full occupancy of the amino ketone intermediate. B. Deconvoluted ESI-mass spectra of PdxS under long incubation (48 hours with 25 mM R5P) yields the observances of a second adduct.

A.

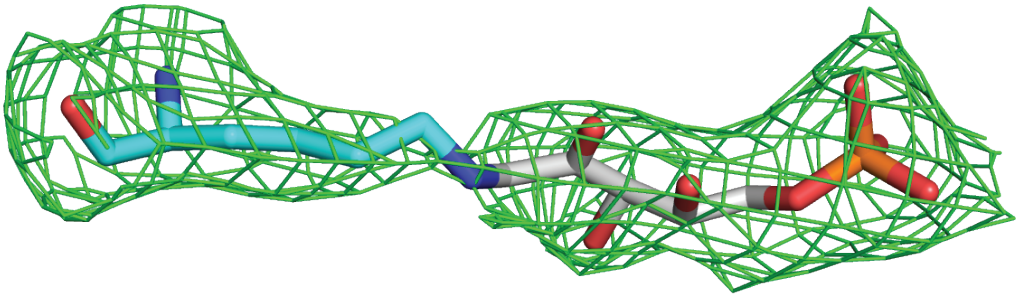

B.

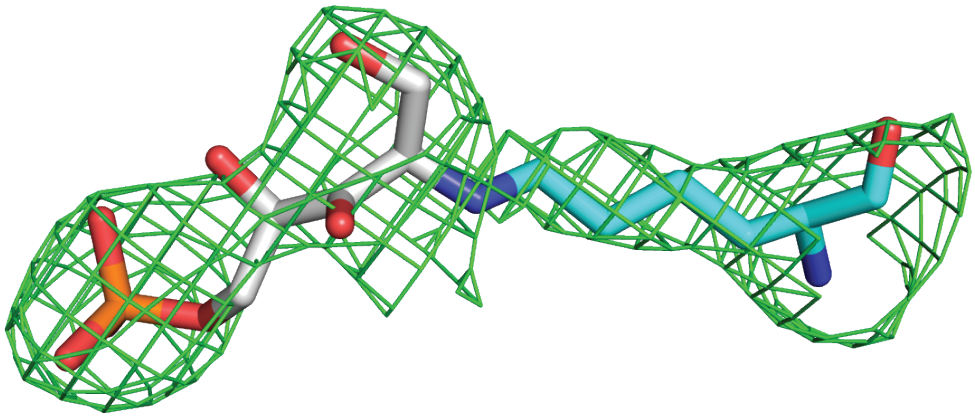

Figure 2.9 R5P adduct at Lys81 through C1 (R5P; gray sticks, Lys81; cyan sticks, F_o-F_c omit density contoured at 2 σ, green). 5RP adduct at Lys149 through C2 (5RP; gray sticks, Lys149; cyan sticks, F_o-F_c omit density contoured at 2 σ, green).

Under the conditions of crystallization, an R5P adduct also formed at Lys149. I observed the doubly modified state in solution upon long-term incubation of PdxS with an excess of R5P (Fig. 2.8B). Density for the adduct at Lys149 was best fit with a connection to the R5P C2 atom (Fig. 2.9B). In refinement tests, the 2-amino, 3-keto isomer at C2 (1-hydroxyl, 2-amino, 3-keto) was a better fit to density than were either the imine at C2 or the alternative amino-ketone at C2 (1-

al, 2-amino, 3-hydroxyl). When an R5P covalent intermediate was discovered[40], Lys149 was identified as the site of the R5P adduct, but the site was reassigned to Lys81 in light of a structure of PLPS co-crystallized with R5P[49]. The Lys149 adduct is unlikely to be on the reaction pathway given its long formation time. Lys149 is at the top of strand β6 in the PdxS β_8/α_8 barrel with the side chain and R5P adduct directed outside the barrel away from the active site. Interestingly, in this position the adduct phosphate occupies an identical site as the phosphate of product PLP in a crystal structure of the yeast enzyme[50] and a phosphate ion in the structure of the PdxS free enzyme[48] (Fig. 2.11). The phosphate has ionic contacts with Arg137 and Arg138, which is positioned in an extensive salt bridge network with Glu103, Lys118 and Glu141. Catalysis was modestly affected by mutagenesis of each Arg, but double substitutions with Gln or Ala reduced activity tenfold (Table 2.6). In contrast, substitutions at Lys149 were deleterious to chromophore formation, and no PLP was formed without a positive charge at this position. Glu103 was the only residue in the salt bridge network where substitutions maintained wild type levels of chromophore formation, although PLP synthesis was reduced four-fold. The C3 hydroxyl forms a hydrogen bond to a conserved Arg130, and the C4 hydroxyl to conserved His115. Substitutions at Arg130 had an effect on both chromophore and PLP formation, while disrupting the hydrogen bonding ability at position 115 decreased PLP synthesis modestly (Table 2.6).

A.

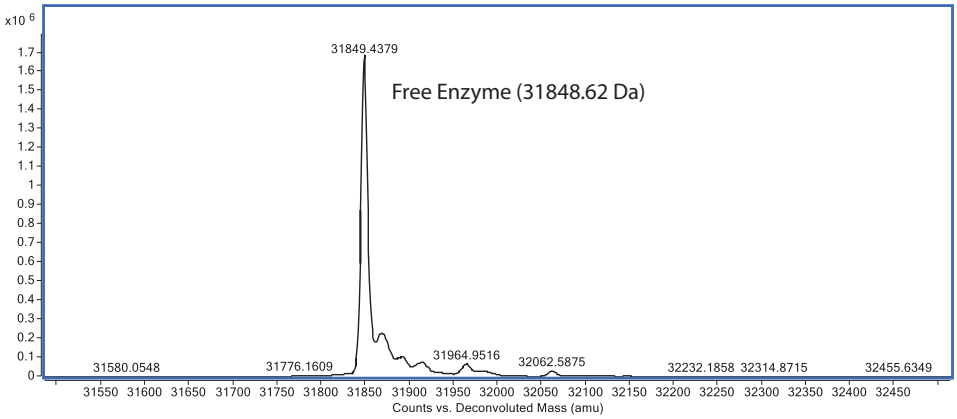

B.

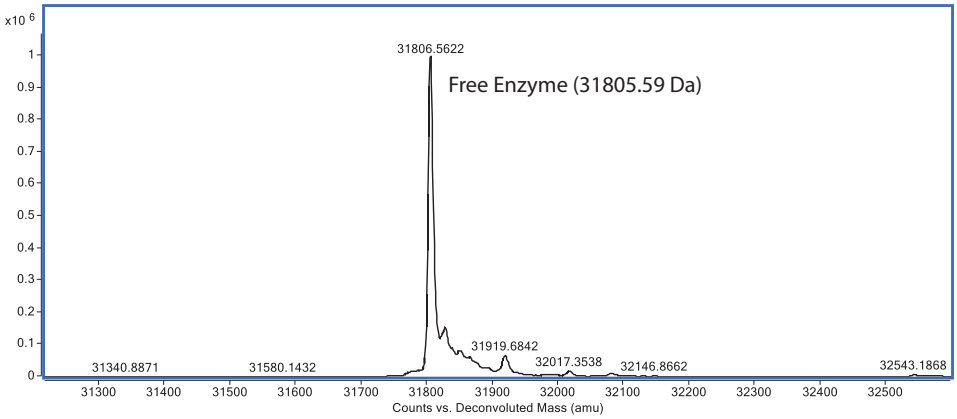

Figure 2.10 Substitutions at Asp24 prevent the accumulation of any R5P adduct. A: D24N B: D24A. Spectra are deconvoluted ESI-mass specta.

Table 2:6 Initial velocity as percent wild type for PdxS variants.

PdxS Variant	Chromophore Formation (initial velocity as % WT)	PLP Synthesis (initial velocity as % WT)
D24N	2 ± 0.9	3 ± 0.5
D24A	N.D.	5 ± 0.5
D102A	118 ± 5	165 ± 3.3
E103Q	97 ± 1	24 ± 1.2
E103A	103 ± 1	23 ± 10.3
H115Q	127 ± 2	78 ± 4.7
H115A	82 ± 0.6	38 ± 1.3
R130Q	18 ± 0.5	57 ± 6.5
R130A	39 ± 0.3	56 ± 2.3
R137Q	16 ± 0.9	34 ± 4.7
R137A	24 ± 0.5	53 ± 2.7
R138K	92 ± 0.9	61 ± 2
R138E	30 ± 0.6	38 ± 2.6
R138Q	25 ± 0.8	33 ± 0.8
R138A	23 ± 0.6	31 ± 0.5
R137QR138Q	6 ± 0.8	10 ± 1
R137AR137A	9 ± 1	16 ± 1.5
R147K	2 ± 1	4 ± 0.5
R147Q	0.8 ± 2.4	4 ± 3.2
R147A	4 ± 1.9	3 ± 2
K149R	4 ± 0.03	9 ± 2.3
K149Q	1 ± 0.2	N.D.
K149A	1 ± 0.1	N.D.

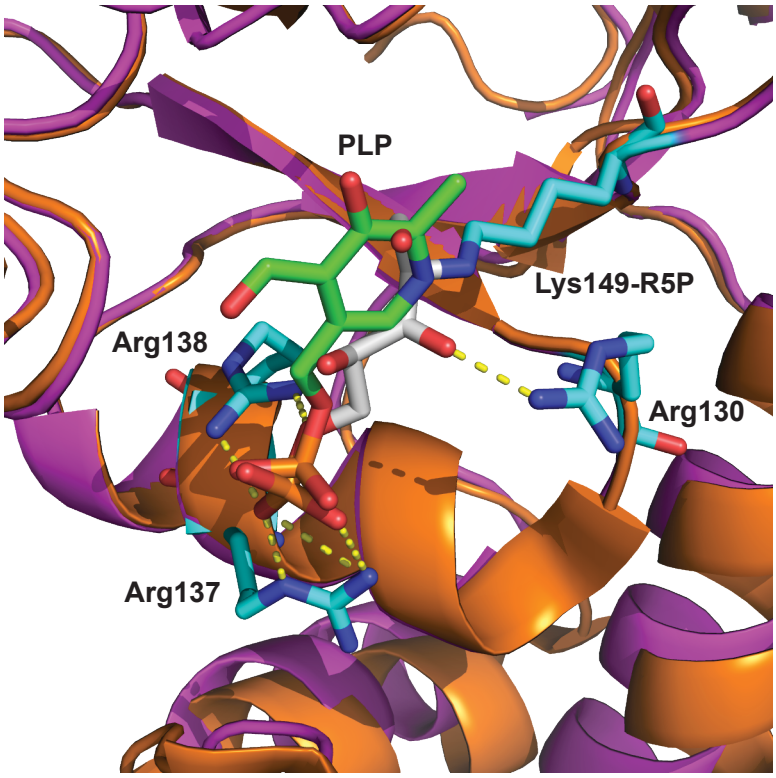

Figure 2.11 Second phosphate binding site. Superposition of *S. cerevisiae* Snz1 structure (orange) with bound PLP (the product, green sticks) and *G. stearothermophilus* PdxS structure (magenta) with bound 5RP (gray sticks) and interacting residues (cyan sticks, yellow dashes).

Second Covalent Intermediate: Amino ketone is converted to the chromophore.

A chromophoric intermediate forms in the PdxS active site when ammonia encounters the R5P covalent intermediate[54,55]. This can be accomplished by addition of glutamine to PLPS or by addition of ammonia to PdxS or PLPS. The chromophore adduct has a mass consistent with addition of NH_2 to the R5P adduct, loss of phosphate and two waters[54,55]. I used intact-protein MS to identify conditions with maximum accumulation of the chromophore in either PdxS or PLPS, but all conditions yielded mixtures of the chromophoric intermediate, the R5P adduct and the free enzyme. Under no conditions was the chromophoric

intermediate the dominant species (Fig 2.12), consistent with previous results[54].

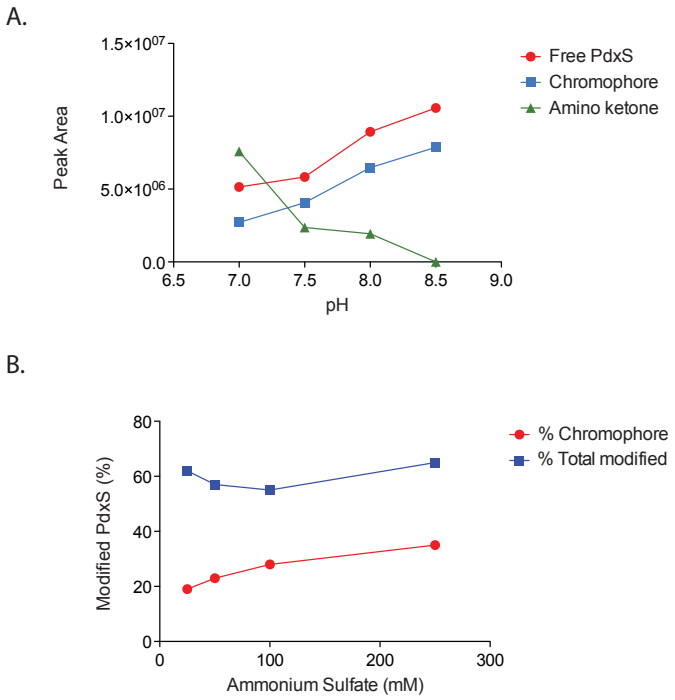

Figure 2.12 Chromophore accumulation. A. Buffers with various pHs were tested in an attempt to maximize the amount of chromophore. Peak areas are from maximum entropy deconvoluted spectra. B. Various ammonium sulfate concentrations were tested at pH 7 in an attempt to maximize the amount of chromophore. Peak areas are from deconvoluted ESI-mass spectra.

I was unable to obtain a structure of PLPS with the chromophore, but replacement of Li citrate with ammonium citrate in the crystallization for the PdxS/R5P structure produced crystals of PdxS in a different form (Fig. 2.13). In this new crystal form, the twelve subunits in the crystallographic asymmetric unit include three states of the synthase active site: R5P adduct, chromophore and no adduct (Fig. 2.14). The density for the covalent adducts is poorer than for the surrounding protein, probably due to a mixture of states in each subunit. The 2.3 Å

structure is a snapshot of PdxS in transition between the Schiff base/amino ketone intermediate and the chromophore intermediate.

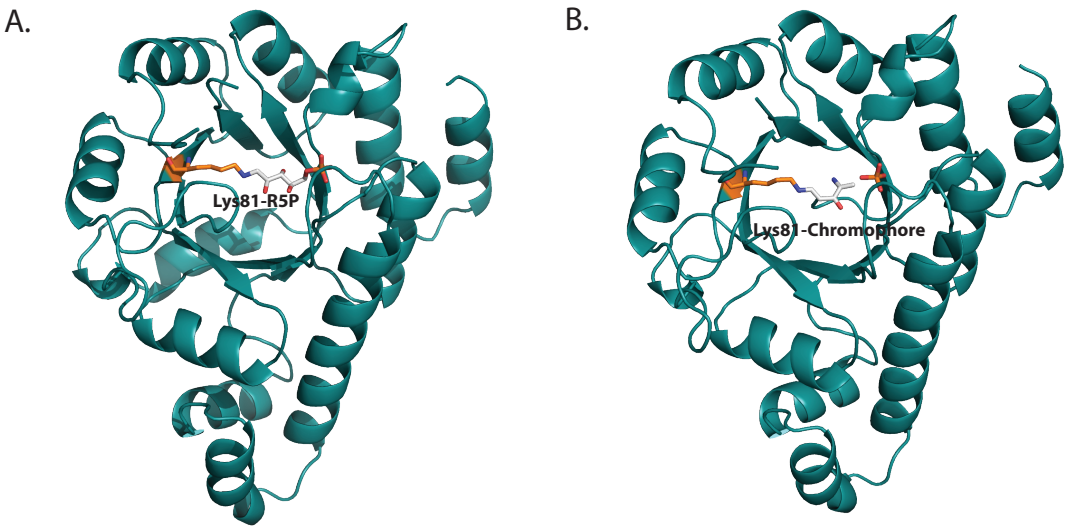

Figure 2.13 PdxS co-crystallized with R5P in the presence of NH_3 contains 3 different substrate species in the 12 active sites of the asymmetric unit. A. Monomer containing the amino ketone. B. Monomer containing the chromophore.

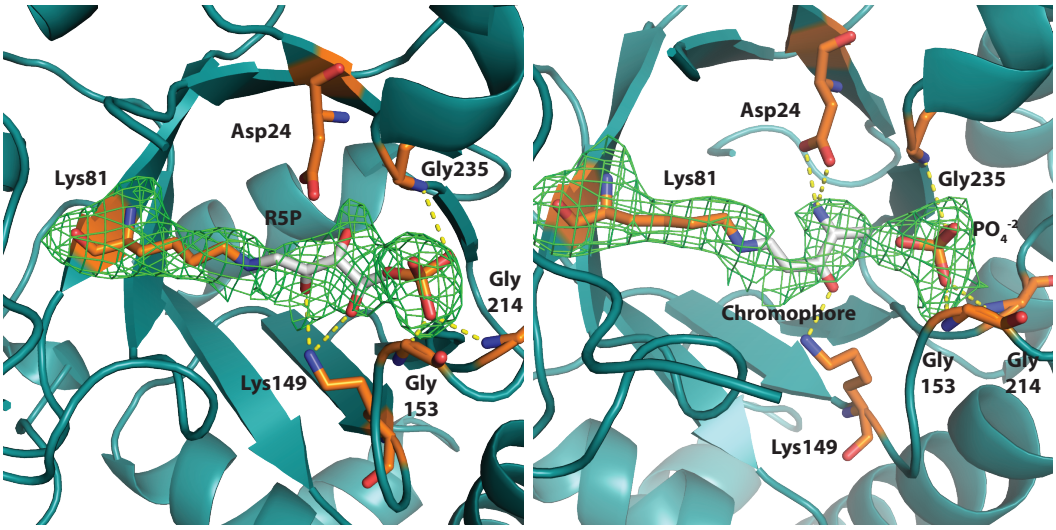

Figure 2.14 Amino ketone intermediate and chromophore intermediate interactions with PdxS. Left: The amino ketone intermediate (gray sticks) at Lys81 (orange sticks; residues that interact with the amino ketone; orange sticks, green; F_o-F_c omit density contoured at 2σ). Right: The chromophore (gray sticks) at Lys149 (orange sticks; residues that interact with the chromophore; orange sticks, green; F_o-F_c omit density contoured at 2σ).

The R5P adduct is the dominant species observed in this structure. Seven of the twelve active sites contain density for the pentulose phosphate amino ketone intermediate at Lys81, two contain density for a phosphate ion, two contain density for the chromophore with density for a free phosphate ion and the remaining active site contains density consistent with five carbon atoms not covalently attached to Lys81 and a free phosphate ion (Fig. 2.14). Density interpreted as the chromophore is consistent with the length of a five-carbon planar adduct. The phosphate ion is clearly separated from the chromophore and remains bound to the same residues that interact with the phosphate group when it is still attached to the amino ketone intermediate.

R5P interacts with PdxS with many of the same residues observed in the

amino ketone structure. In addition to Asp24, Arg147 and Glu102 are conserved and form a salt bridge under the adduct. Substitutions were made at each position and synthase activity was assayed. Substitutions at Asp102 had a negligible effect on either synthase activities (Table 2.6). On the other hand, mutagenesis of Arg147 reduced chromophore formation and PLP synthesis 100-fold. Intact-protein MS revealed that Arg147 substitutions prevented accumulation of the chromophore (Fig. 2.15). The free phosphate is bound through hydrogen bonds with the backbone nitrogens of Gly153, Gly235 and Gly214. In contrast to the structure of the first covalent intermediate, Lys149 points into the R5P active site to hydrogen bond with the C2 hydroxyl of the amino ketone intermediate or the C3 hydroxyl of the chromophore intermediate (Fig. 2.16).

A.

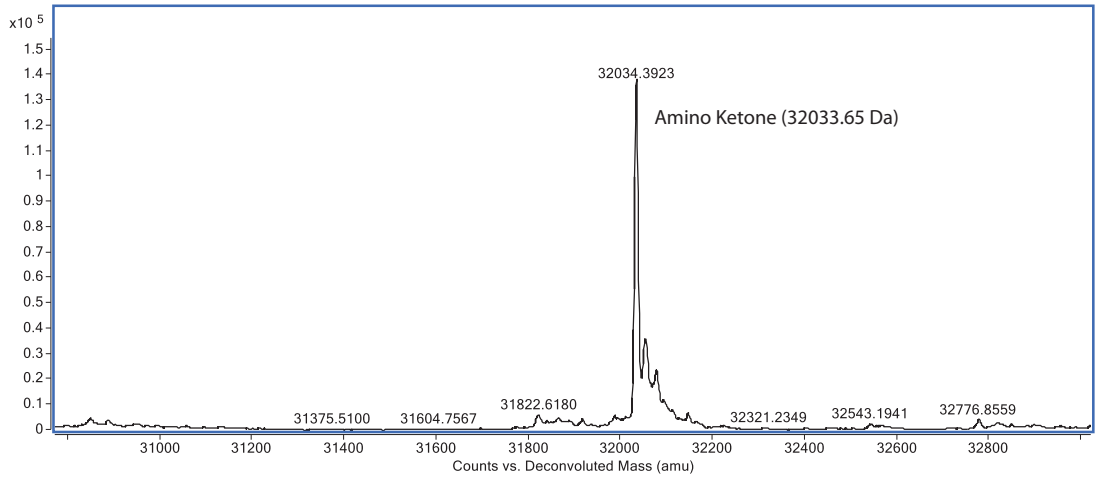

B.

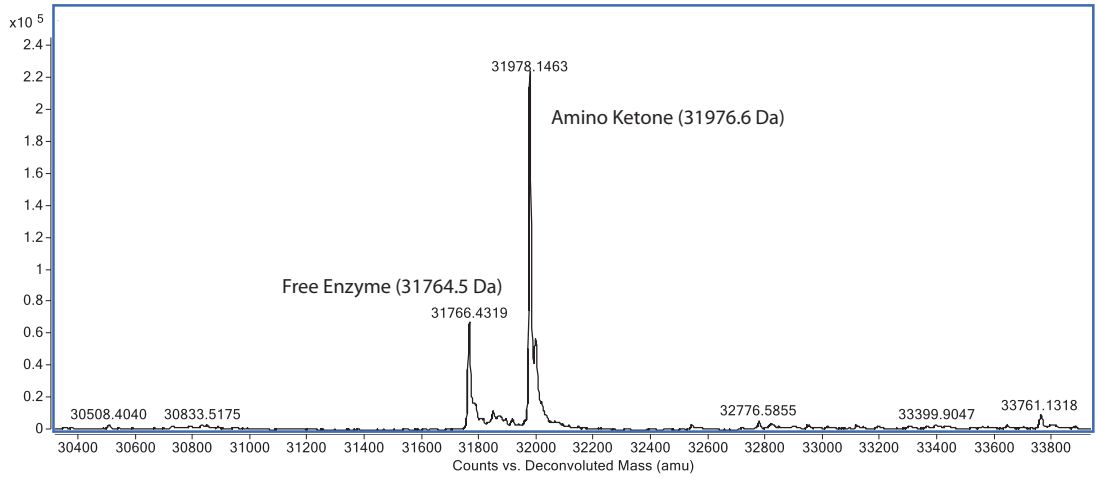

Figure 2.15 Substitutions at Arg147 prevent the formation of the chromophore. A: R147Q B: R147A. Spectra are deconvoluted ESI-mass specta.

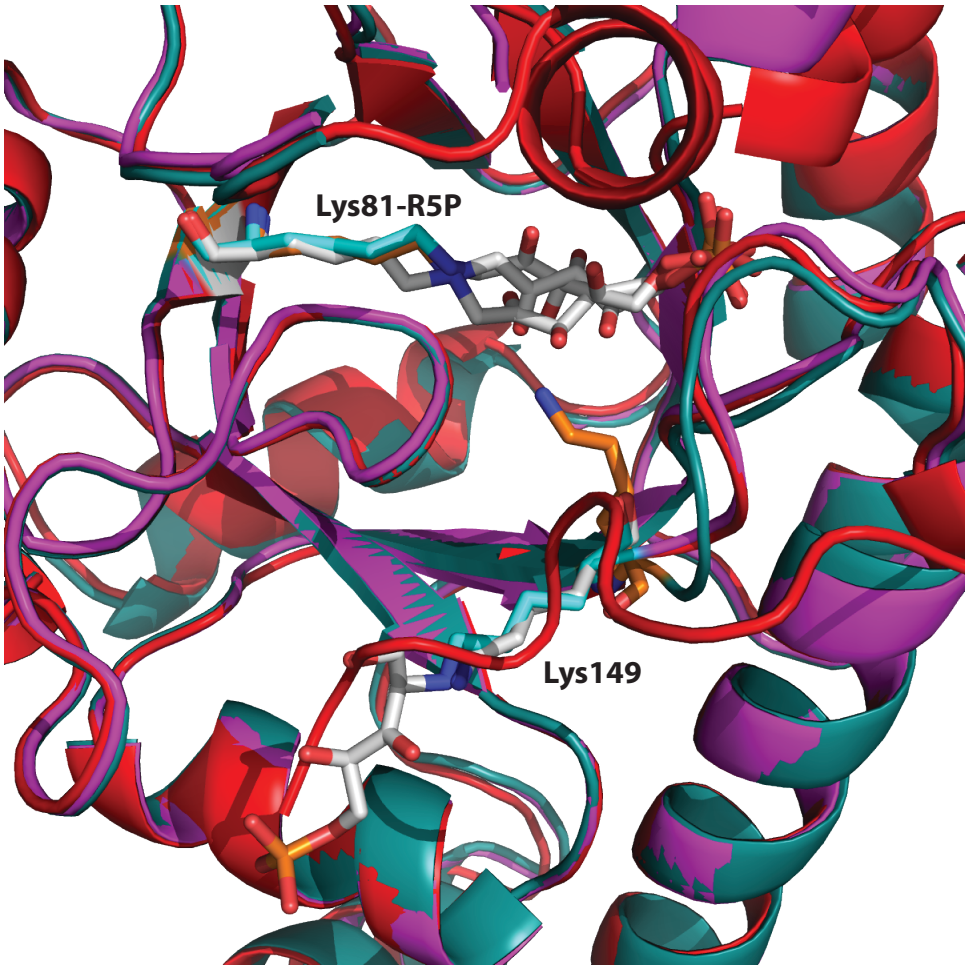

Figure 2.16 Lys149 located on the invariant KGEPG loop in is a different position in the PdxS/R5P/NH_3 structure than its position in any previously solved structures. (PdxS/R5P; magenta/cyan, PLPS TH169N Gln/R5P; red/gray, PdxS/R5P/NH_3; teal/orange).

Discussion

The studies reported in this chapter provide a deeper glimpse into the complex mechanism of the synthase subunit of PLPS. Covalently trapping each synthase intermediate provided snap-shots of the synthase subunit throughout parts of its catalytic cycle. From these structures I was able to observe the structural changes induced by the formation of each adduct within an enzyme from

a single organism and to elucidate the residues necessary to convert the amino ketone to the chromophore. Many mechanistic schemes have been proposed for the conversion of the amino ketone to the chromophore. Understanding how many individual observations fit together has been challenging. The results have given rise to three hypotheses: 1. Dissociation of the covalent intermediate after amino ketone formation followed by reattachment before chromophore formation[56], 2. A second phosphate-binding site outside of the β_8/α_8 barrel[102], and 3. A G3P binding site at the interface between monomers[50]. In order to test these hypotheses I sought to identify structural elements that are critical for specific steps in the synthase mechanism.

Based on the results I propose that the mechanism of PdxS is an all or nothing type reaction, where all the reactions necessary to convert the amino ketone to chromophore happen simultaneously instead of in succession. The structure of the amino ketone and reactivity of ammonia allow for a domino affect to occur that collapses the amino ketone to the chromophore with little catalytic assistance from the enzyme. This hypothesis is based on the inability to trap novel intermediates expected to be stable based on the proposed mechanisms[56]. Potential catalytic residues surrounding the R5P active site include Asp24, Asp102, Arg147 and Lys149 (in the case for the PdxS/R5P/NH_3 structure when Lys149 is pointed into the active site). Among these residues, Asp24, Arg147 and Lys149 had an effect on synthase activities. Substitutions at Asp24 prevented the formation of the amino ketone intermediate suggesting that Asp24 participates in the formation of the Schiff base and its isomerization to the amino ketone.

Substitutions at Arg147 terminated the pathway after amino ketone formation supporting its role in dehydration reactions.

The role of Lys149 is not obvious although others and I have found that it is critical for chromophore and PLP formation[49]. The PdxS/R5P/NH_3 structure is the first instance where Lys149 is pointed into the active site (Fig. 2.16), in all other cases this lysine is outside of the active site[9,48-50]. Two roles can be proposed for Lys149. The first is participation in the conversion of the amino ketone to the chromophore. It was proposed that the amino ketone adduct experiences a C-N bond shift that switches the Lys81 attachment from a C1 to C5 (Fig. 2.17)[56]. The movement of Lys149 may be induced by the presence of NH_3 in the crystallization condition triggering its position within the active site and its participation in the proposed C-N bond flip. Among the twelve active sites one contains density consistent with five carbon atoms detached from Lys81 and a free phosphate ion. The second potential role involves the second observed phosphate site outside the active site where it may be an initial binding site for G3P. Substitutions at Lys149 significantly affected the rate of both synthase activities (chromophore formation and PLP synthesis) supporting a dual purpose.

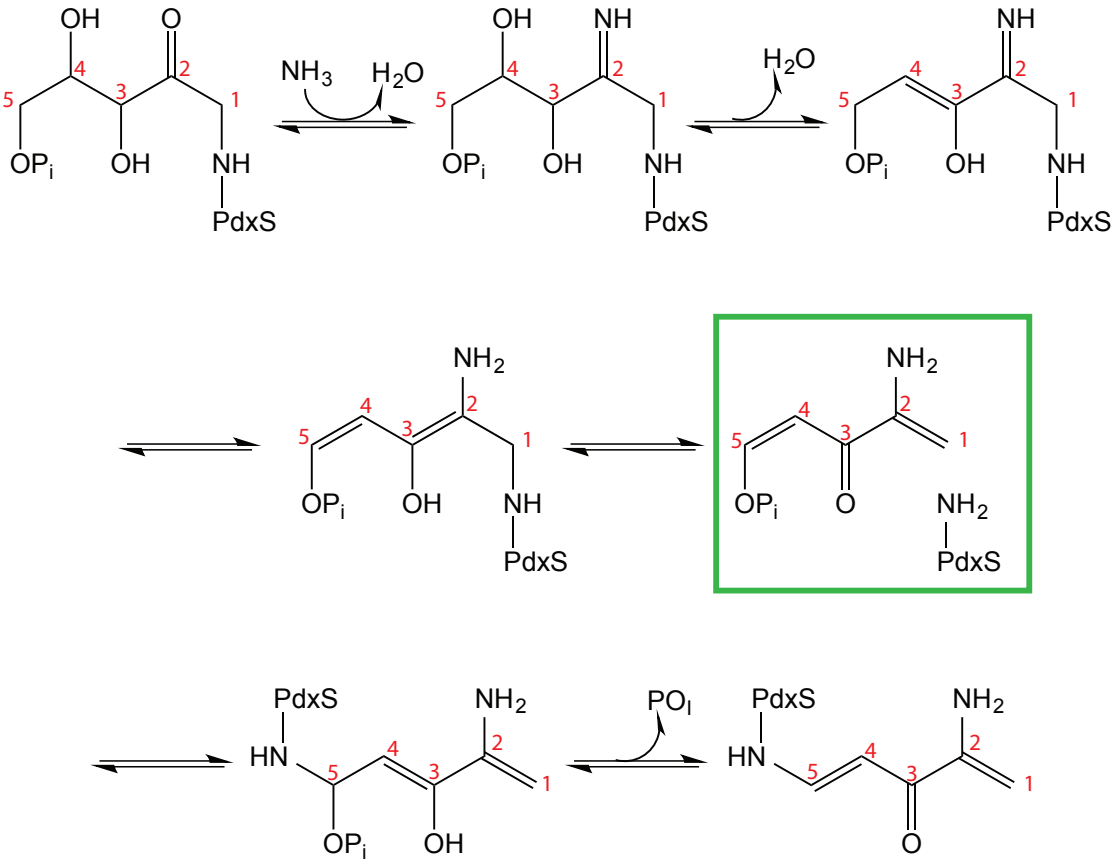

Figure 2.17 Proposed C-N bond shift. NMR results suggest that there is a bond shift during catalysis shifting from a C1 attachment for the amino ketone and a C5 attachment for the chromophore (green box)[56].

Based on the synthase structures, I propose two potential binding sites for G3P. The first site would be with the G3P phosphate replacing the phosphate ion released by chromophore formation (hydrogen bonds to Gly 153, Gly214, and Gly235). The free phosphate ion in the active sites with the chromophore remains bound to the same residues that interact with the phosphate group of the amino ketone intermediate suggesting that the chromophore could be bound at the same time that another phosphate group is bound to the P-loop. Positioning G3P in

proximity to the chromophore should be sufficient for the combination of the two to form PLP. I attempted to find amino acid substitutions that would support chromophore formation but block PLP formation, but no conserved residue at the active site had this property.

A second more interesting hypothesis for G3P binding is that G3P forms a Schiff base with the invariant Lys149 and cradles in the conserved second phosphate binding site outside of the R5P active site. There are many lines of evidence that support the binding site of the second molecule of R5P as a site for G3P binding. First the modification made to Lys149 is a C2 attachment supporting the binding of a shorter molecule than R5P (Fig. 2.18). Phosphate groups, and sulfate ions are prone to bind to this region (Fig. 2.19)[48-50]. Refinement tests supported the attachment at Lys149 as the 2-amino, 3-keto isomer (1-hydroxyl, 2-amino, 3-keto), consistent with the structure of G3P attached at C1. The residues surrounding this site are conserved and there is an extensive salt bridge and hydrogen bond network that propagates from the core of the enzyme to orient the residues directly interacting with this second molecule of 5RP. Substitutions at positions 103 and 115 separate the efficacy of chromophore formation from PLP synthesis suggesting that these residues are important for the binding/incorporation of G3P. The movement of Lys149 into the active site in the presence of NH_3 provides the orientation and proximity necessary for the incorporation into the chromophore adduct in addition to sequestering G3P, which has a higher K_m than the other two substrates.

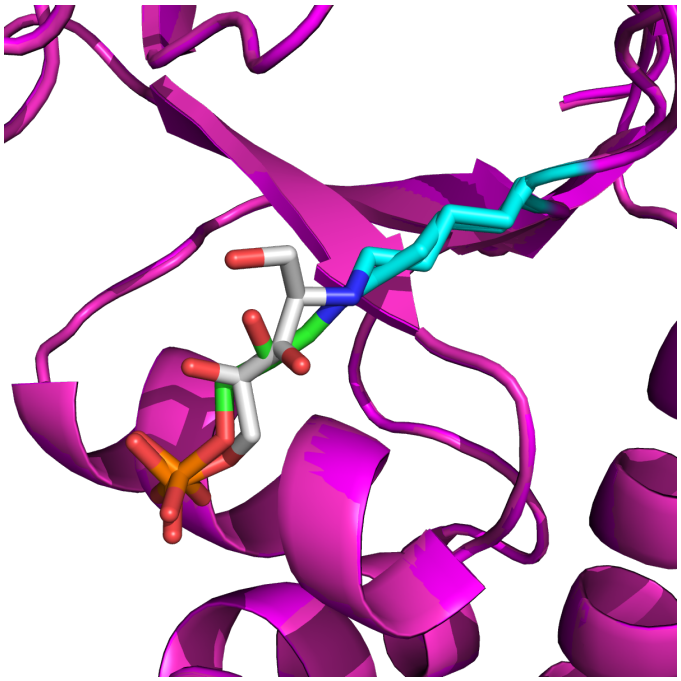

Figure 2.18 Modeled Lys149-G3P adduct. G3P (green sticks) modeled on Lys149 (cyan sticks), the phosphate group is in the same position as the C2 5RP covalent adduct.

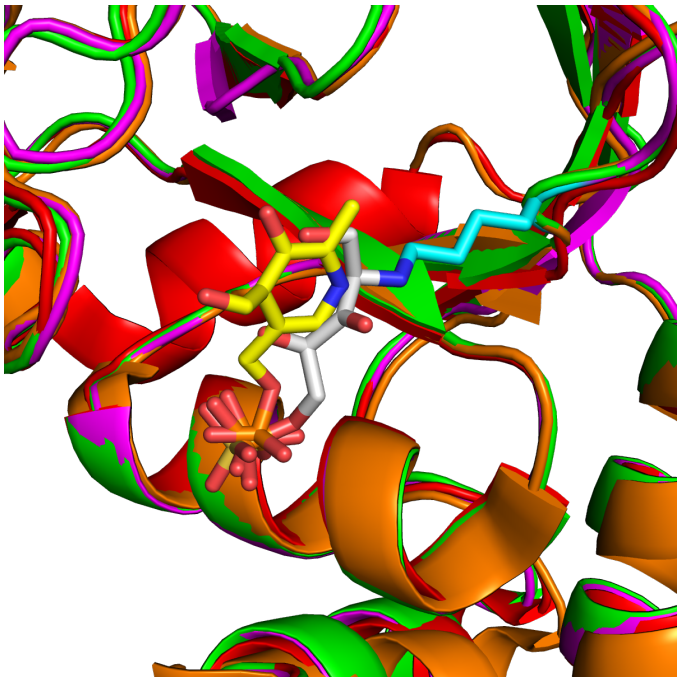

Figure 2.19 Superposition of the second phosphate-binding site. Superposition of *G. stearothermophilus* PdxS/R5P/NH_3 (cyan/gray sticks, magenta), *S. cerevisiae* Snz1/PLP (yellow sticks; PDB: 3O05; orange), *T. maritima* PLPS/R5P/PO_4^{-3} (PDB: 2ISS; red) and *G. stearothermophilus* PdxS/SO_4^{-2} (PDB: 1ZNN; green). All of the sulfate and phosphate groups bind to the second phosphate-binding site.

Overall, I propose that formation of the amino ketone and the chromophore are the only steps in the synthase mechanism that require catalytic residues (Lys81, Asp24 and Arg147). Mutagenesis implicated Lys149 in both synthase activities. These structures reveal that Lys149 is dynamic. The position of Lys149 is apparently an effect of ammonia. In the presence of ammonia Lys149 is positioned inside of the R5P active site and interacts with the chromophore. In the absence of ammonia Lys149 is positioned outside of the R5P active site and may form a covalent adduct with G3P. Each position addresses a role for Lys149 in both synthase activities.

I propose two potential binding sites for G3P. The first site, in accord with

the conventional binding sites known to proteins with the β_8/α_8 fold, fits the spatial constraints necessary to incorporate G3P into the chromophore. The second site provides a biological role for the secondary phosphate-binding site and suggests a mechanism that proceeds through two subsequent Schiff bases on different residues (Lys81 and Lys149). Substitutions to residues surrounding the second exterior phosphate-binding site decrease, without abolishing, the efficacy of PLP synthesis. The mutagenesis results suggest that this site is implicated in G3P binding and PLP formation but not involved in chromophore formation. On the other hand, failure to identify residues that eliminate PLP synthesis completely without affecting chromophore formation supports overlapping binding sites for R5P and G3P, and that G3P incorporation does not require catalytic activation.

Chapter 3

The Role of the C-terminal tail of PdxS

Summary

PLP synthase (PLPS) from the bacterium *Geobacillus stearothermophilus* generates pyridoxal 5'-phosphate (PLP), the active form of vitamin B_6, from glutamine, ribose 5-phosphate (R5P) and glyceraldehyde 3-phosphate (G3P). PLPS is a D_6-symmetric complex of 12 synthase subunits (PdxS) and 12 Triad glutaminase subunits (PdxT). PdxS forms a cylindrical dodecamer of two hexameric rings[48]. PdxT binds around the outside of the PdxS stacked rings[49]. Ammonia, generated from glutamine hydrolysis in PdxT, is channeled to the PdxS synthase active site where it joins R5P and G3P to form PLP by an elusive mechanism that proceeds through two sequential covalent intermediates. First, PdxS and R5P form an enzyme-imine[40], which then undergoes isomerization to a stable amino ketone intermediate[56]. Dehydration and conjugation upon incorporation of NH_3 and concomitant loss of inorganic phosphate leads to the generation of a chromophoric adduct[54,55]. Chromophore formation and PLP synthesis are dependent on the presence of the C-terminal tail of PdxS, which is generally disordered[6]. Using an inactive mutant of PdxT, I co-crystallized PLPS with substrates glutamine and R5P. This is the first structure of PLPS with multiple substrates. Initial crystals with d_{min} ~4 Å were improved with dehydration to d_{min} ~ 2.7 Å. The higher resolution structure contains all but four amino acids of the C-terminal tail of PdxS,

consistent with the observed decrease in accessibility of the tail upon substrate binding[6]. The ordered C-terminal tail interacts with the body of the synthase subunit, acting as a shield over the R5P active site in a more closed state of the synthase subunit. Additionally, glutamine and R5P binding initiate conformational changes around the R5P active site that bury R5P into the core of PdxS. Through biochemical assays, I identified conserved charged residues responsible for these movements, suggesting that the closed state is crucial to the formation of the chromophore.

Introduction

Structural studies have been critical in dissecting the mechanism of PLPS and connecting the results derived from biochemical studies to a catalytic mechanism. Structures of the heteromeric PLPS complex and the dodecameric synthase complex have been solved from both prokaryotic and eukaryotic microorganisms, with and without substrates[9,48-50]. All structures solved to date lack any structural information regarding the C-terminal tail of the synthase subunit and contain at most one substrate (Fig. 3.1). The range of missing C-terminal residues ranges from 14-28 amino acids[9,48-50]. The structure of *Thermotoga maritima* PLPS co-crystallized with R5P contains the most C-terminal residues observed in any structure[49]. The increase in order is attributed to the covalent intermediate of the synthase subunit and R5P and additionally the binding of a phosphate ion to a secondary binding site on the synthase subunit[49]. The consistent disorder of the C-terminal tail led to investigation of the importance of this flexible segment for enzyme function[6]. Truncation of these residues abolished both chromophore formation and PLP synthesis[6].

A.

Organism	Subunits	Substrates
Bacillus subtilis	PLPS	glutamine
Saccharomyces cerevisiae	Snz1	PLP
		G3P
Thermotoga maritima	PLPS	R5P

B.

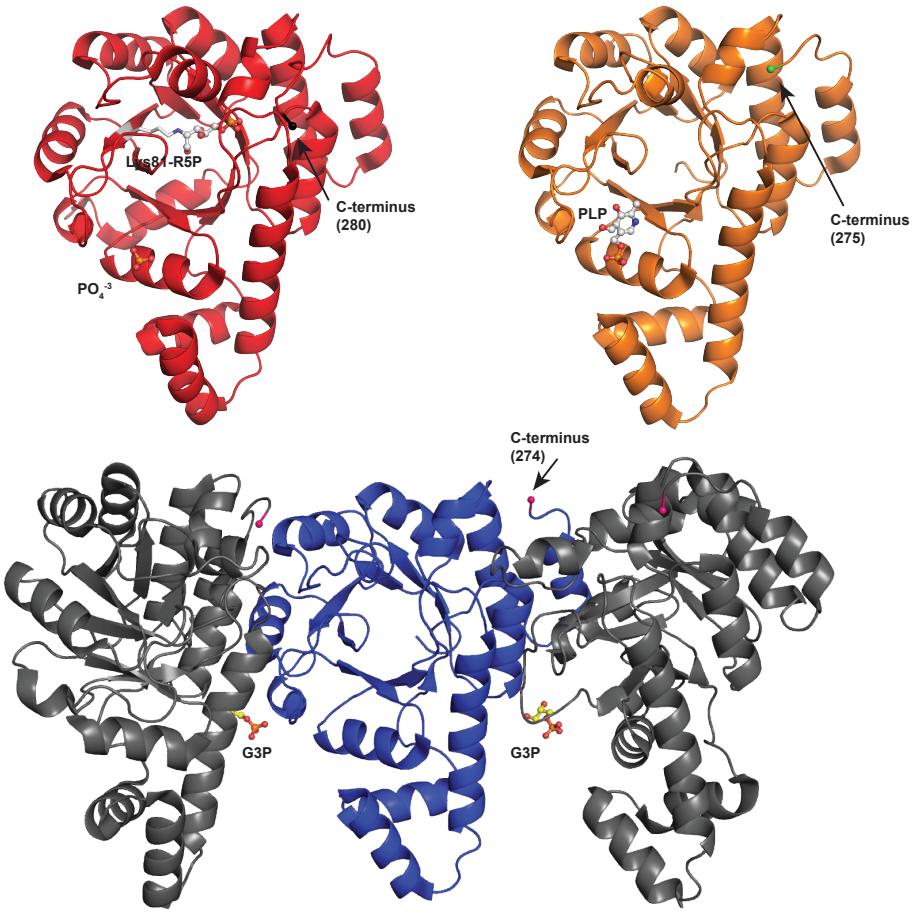

Figure 3.1 The active sites of the synthase subunit. A. Structures from various biological sources have been determined for either the synthase subunit or the intact enzyme (PLPS) with each substrate individually. B. Independent of the substrate or product, the C-terminus of PdxS is disordered (spheres). PLPS from *T. maritima* (synthase subunit; red) with R5P covalently attached (gray spheres)[49]. Synthase subunit from *S. cerevisiae* (orange) with PLP (gray spheres)[50]. Synthase subunit from *S. cerevisiae* (blue/gray) with G3P (yellow sticks)[50].

In order to obtain an understanding of the structural role of the C-terminal tail in regards to the synthase activity, tryptophan quenching and proteolysis experiments were conducted[6]. Tryptophan quenching experiments revealed a decrease in fluorescence in the presence of the glutaminase subunit and a further decrease in the presence of glutamine[6]. Proteolysis experiments revealed that the C-terminal tail is protected from proteolysis in the presence of substrates and that the effect is additive in the presence of the glutaminase subunit and both acceptor substrates[6]. These results suggest that the synthase C-terminal tail becomes ordered in the presence of the glutaminase subunit and substrates, behaving in a manner similar to a lid[6].

Our objective was to crystallize *Geobacillus stearothermophilus* PLPS with an ordered C-terminal tail. In order to accomplish this, based on previously published data, PLPS would need to be crystallized with as many substrates bound as possible. To trap glutamine, the catalytic histidine (169) was mutated to an asparagine preventing the release of glutamate, locking the glutaminase in a acyl-enzyme intermediate (Fig. 3.2)[9]. Covalent attachment of R5P to PdxS is independent of the remaining substrates or the glutaminase subunit. Therefore, the ability to co-crystallize PLPS with at least two substrates using the inactive glutaminase mutant in the presence of glutamine and R5P should order the C-terminal tail of PdxS. My hypothesis is that co-crystallization of PLPS/H169N_T with glutamine and R5P will provide structural information regarding the position of the C-terminal tail and its role in chromophore formation and PLP synthesis. I expressed PLPS with the inactive glutaminase mutant (PdxT/H169N) and co-crystallized PLPS in the presence of Gln and R5P. This is the first structure of PLPS

from *G. stearothermophilus* and the first structure of PLPS with more than one bound substrate.

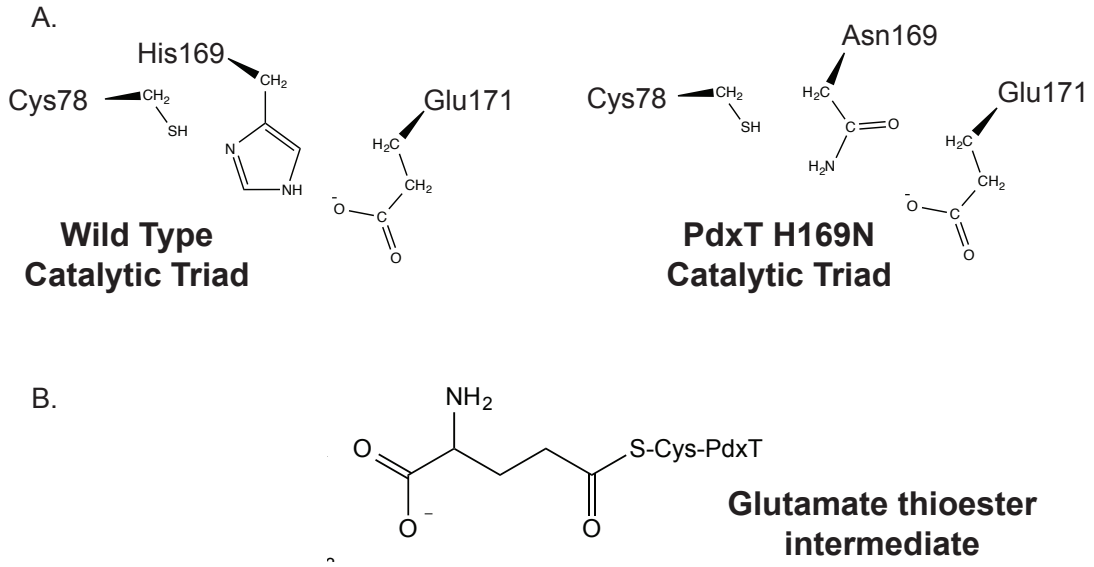

Figure 3.2 Glutaminase inactive variant. A. Mutating the catalytic histidine to an asparagine prevents the release of glutamate. B. PdxT H169N locks the glutamyl thioester intermediate on the nucleophilic cysteine.

Experimental Procedures

Cloning of G. stearothermophilus *pdxS* and *pdxT*-

The plasmids pET0881[48] for PdxS and pET0669[103] for PdxT were used for all mutagenesis and sub-cloning. PdxT H169N and some substitutions in PdxS (R53K, R53E, R53A, R53Q, E151S, E151A, E151Q, R288K, R288E, R288Q and R288A) were generated by site directed mutagenesis (SDM) (QuikChange by Strategene). Primers are listed in Table 3.1. PdxS truncations and substitutions made at 291 and 292 were generated by sub-cloning, followed by insertion into an appropriate expression vector

using ligation independent cloning (LIC)[104]. Primers and expression vectors are listed in Table 3.2.

Table 3:1 Primers and expression vectors for constructs generated by SDM.

Primers for SDM				
Plasmid Name	**Mutation**	**Expression Vector**	**Direction**	**Primer**
pET0669_H169N	PdxT H169N	pET281	Forward	5'-TCGGCTGCTCGTTC**AAT**CCAGAGCTGACC-3'
pET0881_R53K	PdxS R53K	pET281	Forward	5'-GCGCGTCCCGGCGGACATT**AAG**GCCGCTGGCG-3'
pET0881_R53E	PdxS R53E	pET281	Forward	5'-GCGTCCCGGCGGACATT**GAG**GCCGCTGGC-3'
pET0881_R53A	PdxS R53A	pET281	Forward	5'-GCGTCCCGGCGGACATT**GCC**GCCGCTGG-3'
pET0881_R53Q	PdxS R53Q	pET281	Forward	5'-CCGGCGGACATT**CAG**GCCGCTGGCGGT-3'
pET0881_E151S	PdxS E151S	pET281	Forward	5'-TCGATGTTGCGGACGAAAGGA**TCG**CCGGGGACAG-3'
pET0881_E151A	PdxS E151A	pET281	Forward	5'-GGACGAAAGGA**GCG**CCGGGGACAGG-3'
pET0881_E151Q	PdxS E151Q	pET281	Forward	5'-TGTTGCGGACGAAAGGA**CAG**CCGGGGA-3'
pET0881_R288K	PdxS R288K	pET281	Forward	5'-ATTGTTGCCGGAGCAC**AAG**ATGCAAGAACGCGGC-3'
pET0881_R288E	PdxS R288E	pET281	Forward	5'-TTGTTGCCGGAGCAC**GAG**ATGCAAGAACGCGG-3'
pET0881_R288Q	PdxS R288Q	pET281	Forward	5'-GTTGCCGGAGCAC**CAG**ATGCAAGAACGCG-3'
pET0881_R288A	PdxS R288A	pET281	Forward	5'-TGTTGCCGGAGCAC**GCG**ATGCAAGAACGCG-3'

Table 3:2 Primers and expression vectors for constructs generated by sub-cloning and LIC.

Primers for LIC						
Plasmid Name	**Start**	**End**	**Mutation**	**Expression Vector**	**Direction**	**Primer**
PdxS START 3					Forward	5'-TACTTCCAATCCAATGCAAGCACAGGTACGGAC-3'
pPdxSTail_270	3	270		pMCSG 7	Reverse	5'-TTATCCACTTCCAATGTTATCCTTTCGACAAGTGTGC-3'
pPdxSTail_278	3	278		pMCSG 7	Reverse	5'-TTATCCACTTCCAATGTTAGATGCCGCGCATCG-3'
pPdxSTail_286	3	286		pMCSG 7	Reverse	5'-TTATCCACTTCCAATGTTACTCCGGCAACAATGTC-3'
pPdxSTail_290	3	290		pMCSG 7	Reverse	5'-TTATCCACTTCCAATGTTATTGCATCCGGTGCT-3'
pPdxSTail_293	3	293		pMCSG 7	Reverse	5'-TTATCCACTTCCAATGTTAGCCGCGTTCTTGC-3'
pPdxS_E291D	3		PdxS E291D	pMCSG 7	Reverse	5'-TTATCCACTTCCAATGTTACCAGCCGCGGTCTTGC-3'
pPdxS_E291Q	3		PdxS E291Q	pMCSG 7	Reverse	5'-TTATCCACTTCCAATGTTACCAGCCGCGTTGTTGC-3'
pPdxS_E291A	3		PdxS E291A	pMCSG 7	Reverse	5'-TTATCCACTTCCAATGTTACCAGCCGCGTGCTTGC-3'
pPdxS_R292K	3		PdxS R292K	pMCSG 7	Reverse	5'-TTATCCACTTCCAATGTTACCAGCCTTTTTCTTGCATCCGGTG-3'
pPdxS_R292E	3		PdxS R292E	pMCSG 7	Reverse	5'-TTATCCACTTCCAATGTTACCAGCCTTCTTCTTGCATCCGGTG-3'
pPdxS_R292Q	3		PdxS R292Q	pMCSG 7	Reverse	5'-TTATCCACTTCCAATGTTACCAGCCCTGTTCTTGCATCCG-3'
pPdxS_R292A	3		PdxS R292A	pMCSG 7	Reverse	5'-TTATCCACTTCCAATGTTACCAGCCTGCTTCTTGCATCCGGT-3'

Expression and Purification of PdxS and PdxT:

PdxS and PdxT were expressed and purified separately. Cells of *E. coli* strain BL21(DE3) were transformed with the appropriate expression plasmid, grown at 37°C in Luria-Bertani (LB) medium until OD_{600} reached 0.8. The temperature was reduced to 20°C for 1 hr, expression was induced with 400 μM isopropyl β-D-thiogalactopyranoside (IPTG), and cultures were incubated 12-16 hr. All purification steps were carried out at 4°C unless otherwise noted. Cells from a 1L culture were harvested by centrifugation,

re-suspended in 40 mL of Buffer A (20 mM Tris-HCl pH 7.9, 500 mM NaCl), lysed by sonication, and centrifuged at 18,000 x g. The supernatant was filtered and loaded onto a Ni^{+2} affinity column (HisTrap^{TM}HP, GE Healthcare). Bound protein was eluted with a linear gradient of 0-500 mM imidazole in Buffer A. The N-terminal His_6-tag of PdxS was removed by TEV protease by 4 hr digestion at room temperature followed by dialysis (Buffer A). TEV protease and un-cleaved PdxS were removed by Ni^{+2} affinity chromatography. Proteins intended for crystallization were further purified by gel filtration. PdxS was purified on an S300 column (HiPrep^{TM} 16/60 Sephacryl^{TM} S-300 HR, GE Healthcare) using 20 mM Tris-HCl pH 8.5, 500 mM NaCl, 10 mM glutamine, 2 mM DTT. PdxT was purified on an S100 column (HiPrep^{TM} 16/60 Sephacryl^{TM} S-100 HR, GE Healthcare) using 20 mM Tris-HCl pH 7.9, 500 mM NaCl, 2 mM DTT. Intact PLPS was reconstituted by mixing PdxS and PdxT H169N in a 2:3 ratio in the presence of 10 mM glutamine, purified by gel filtration (S300 column with 20 mM Tris-HCl pH 7.9, 500 mM NaCl, 10 mM glutamine, 2 mM DTT), dialyzed (20 mM Tris-HCl pH 7.9, 10 mM glutamine) and stored at -80^{O}C.

PLPS Activity Assays:

Glutaminase activity was assayed using a coupled reaction with glutamate dehydrogenase (GDH)[8]. Reactions were carried out at 37°C in a total reaction volume of 250 µL containing 50 µM PdxS, 50 µM PdxT, 100 mM Tris-HCl pH 8.5, 20 mM glutamine, 50 mM KCl, 0.375 mM 3-acetylpyridine adenine dinucleotide ($APAD^+$) and 1.8 µM GDH (Sigma). Glutamate formation was monitored by GDH reduction of $APAD^+$ to APADH detected at 363 nm using a SpectraMax M5 Multi-Mode Microplate Reader (Molecular Devices).

Formation of the chromophoric adduct of R5P and NH_3 with PdxS was assayed at 37°C in a total reaction volume of 50 µL containing 50 µM PdxS, 50 µM PdxT, 50 mM Tris-HCl pH 7.9, 20 mM glutamine or 20mM $(NH_4)SO_4$ and 10mM R5P[55]. The chromophoric adduct was detected by absorbance at 315 nm in a SpectraMax M5.

PLP synthesis was assayed at 37°C in a total reaction volume of 50 µL containing 50 µM PdxS, 50 µM PdxT, 50 mM Tris-HCl pH 7.9, 20 mM glutamine, 10mM R5P, 20 mM G3P. PLP was detected by absorbance at 415 nm in a SpectraMax M5.

For determination of kinetic constants, 1 µM PLPS was used and the reactions were carried out under the conditions stated above.

Crystallization/Dehydration

PLPS/H169N_T/R5P/Gln was crystallized at 20°C by hanging drop vapor diffusion using 1 µL of protein solution (7 mg/mL PLPS/H169N_T, 20 mM Tris-HCl pH 7.9, 5 mM R5P, 10 mM Gln) and 1 µL reservoir solution (14% PEG 3350, 200 mM Na malonate pH 7.0). Crystals appeared within 2 days, grew over 7 days, and were dehydrated by serial transfer of the cover slip to wells containing the original mother liquor with the PEG 3350 concentration increased by 5% every 12 hours to a final concentration of 39%[105]. Crystals were directly flash-cooled in liquid nitrogen. Crystal dehydration resulted in a 14% decrease in the unit cell volume (7,315,128 $Å^3$ to 6,312,125 $Å^3$) and an improvement in the diffraction limit from 3.9 Å to 2.69 Å.

X-ray Data Collection and Processing:

Data were collected at the Advanced Photon Source (APS) at the Argonne National laboratory on the GM/CA beam line 23ID-D. Data were processed and scaled with the HKL2000 suite (Table 3.3)[91]. Summaries of the crystallographic statistics are listed in

Table 3.4. Initial phases for PLPS/R5P/Gln was determined by molecular replacement (MR) using the program BALBES[106] and the structures of PdxS[48] (1ZNN) and PdxT[9] (2NV2). Iterative model building was done in COOT[94] and refinement was carried out with REFMAC[95] and Buster [107]. TLS groups were determined using the webserver TLS MD[96,97]. Link records for PdxS Lys81-R5P and Cys78-Gln were created using J Ligand[98]. The restraints and coordinates for the Schiff base between PdxS Lys 81 and the thioester intermediate between PdxT Cys78 and glutamine (CYQ) were created using prodrg[99] and the grade server[100]. The final model was validated with MolProbity (Fig. 3.3)[101].

Table 3:3 Scaling statistics for PLPS/H169N$_T$/R5P/Gln.

Shell Limit (Å)		Average I	Average Error	Chi^2	Linear R-factor	Multiplicity
Lower	Upper					
50.00	7.32	922.1	66.1	0.526	0.044	3.3
7.32	5.81	295.2	21.9	0.671	0.053	3.4
5.81	5.08	277.9	21.1	0.742	0.060	3.4
5.08	4.62	381.8	29.1	0.888	0.065	3.4
4.62	4.29	363.3	28.0	1.256	0.084	3.4
4.29	4.03	293.5	23.5	1.030	0.083	3.4
4.03	3.83	237.7	20.5	1.067	0.088	3.4
3.83	3.66	191.1	17.8	1.214	0.105	3.4
3.66	3.52	163.7	16.4	1.042	0.111	3.4
3.52	3.40	125.5	14.4	1.083	0.138	3.4
3.40	3.30	105.5	13.4	1.134	0.164	3.3
3.30	3.20	81.5	12.4	1.193	0.208	3.3
3.20	3.12	64.5	11.8	1.174	0.251	3.2
3.12	3.04	57.9	11.7	1.203	0.282	3.2
3.04	2.97	41.8	10.9	1.260	0.381	3.2
2.97	2.91	35.6	10.8	1.250	0.438	3.2
2.91	2.85	33.1	10.8	1.216	0.464	3.2
2.85	2.80	27.9	10.7	1.262	0.560	3.1
2.80	2.75	25.8	10.7	1.240	0.601	3.1
2.75	2.70	22.7	10.7	1.315	0.687	3.1
All Reflections		**188.7**	**18.7**	**1.081**	**0.101**	**3.3**

Table 3:4 Crystallographic data and refinement statistics for PLPS/H169N$_T$/R5P/Gln.

	PLPS/H169N$_T$/R5P/Gln
Diffraction data	
X-ray Source	APS 23ID-D
wavelength	1.033
space group	$C222_1$
unit cell parameters (Å)	141.02, 249.14, 179.66
α, β, γ (°)	90, 90, 90
asymmetric unit	6 PdxS, 6 PdxT/H169N
resolution limit (Å)	2.69 (2.76-2.69)
unique reflections	87355
avg. I/σ_I	15.5(2.1)
avg. redundancy	3.3(3.1)
completeness (%)	98.9(98.9)
R_{sym}	0.101(0.695)
Refinement	
data range	50-2.69
Reflections	81715
R/Rfree (%)	20.9/25.7
RMS deviations	
bonds lengths (Å)	0.0114
bond angles (deg)	1.4022
average B factors (Å^2)	
protein	59.5
water	40.5
ligands	62.7
Ramachandran	
Favored (%)	96.3
Allowed(%)	3.2
Outlier (%)	0.5
Number of Atoms	
Protein	21682
Water	263
Ligands	222

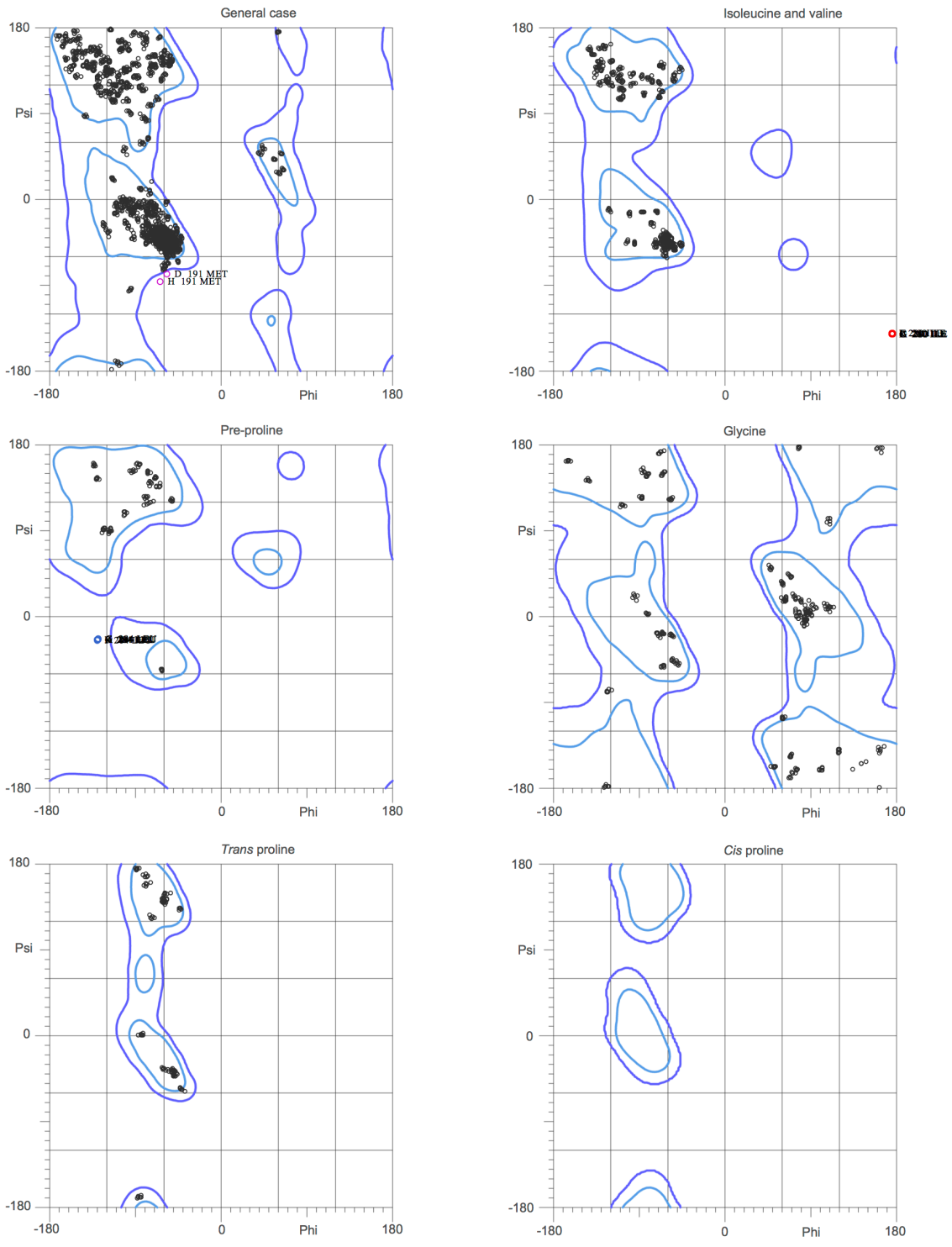

Figure 3.3 Ramachandran plot for PLPS/H169N$_T$/R5P/Gln. Ramachandran plots for PLPS/H169N$_T$/R5P/Gln indicate that 96.4% of all residues were in favored regions and 99.5% of all residues were in allowed regions. Plots were generated using Molprobity[101].

Results

Kinetic characterization of PLPS from *G. stearothermophilus*.

Several assays were used to evaluate PLPS activity, including glutamine hydrolysis by intact PLPS, chromophore formation by PLPS or PdxS, and PLP formation by PLPS and PdxS. Kinetic constants for PLPS were determined for all three substrates (Table 3.5). The K_m values are similar to those published for *Bacillus subtilis* PLPS[8,102]. PLPS displayed Michaelis-Menten behavior with no detectable cooperativity. For most GATs the glutaminase activity is dependent on or accelerated by the synthase substrates[108,109]. This mode of regulation couples the two catalytic activities, efficiently generating ammonia only when the synthase substrates are present, thus preventing wasteful glutamine hydrolysis. In contrast, the glutaminase activity of PLPS was not dependent on or accelerated by R5P or G3P, but was dependent on formation of intact PLPS from the glutaminase subunit (PdxT) and the synthase subunit (PdxS). Under saturating conditions glutamine was hydrolyzed six times more quickly than PLP was synthesized. This discrepancy between the two active sites indicates that the glutaminase active site is not efficiently coupled to the synthase active site. This was previously shown in PLPS from *B. subtilis*[8,9,54], and is confirmed here for PLPS from *G. stearothermophilus.* Although the synthase activities can be reconstituted using ammonia as a nitrogen source, the efficiency is 2-fold lower than with glutamine (Fig. 3.4). This is also the case for Pdx1 from *B. subtilis*[40,55].

Table 3:5 Kinetic constants for PLPS from *G. stearothermophilus.*

Activity	Variable Substrate	K_m (μM)	k_{cat} (μM/min)	k_{cat}/K_m(μmol/min·mM)
glutaminase	glutamine	600 ± 70	0.06 ± 0.001	0.1 ± 0.012
synthase	G3P	1600 ± 400	0.01 ± 0.005	0.0063 ± 0.0016
synthase	R5P	10 ± 2	0.01 ± 0.0003	1 ± 0.2

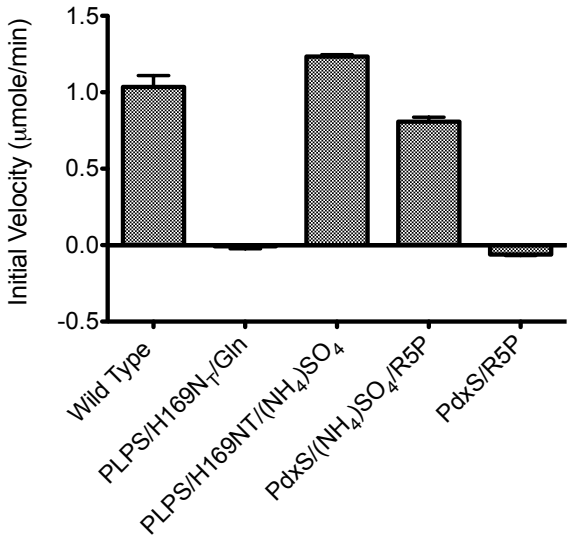

Figure 3.4 Ammonium sulfate can substitute for PdxT and glutamine. Comparing wild type activity for chromophore formation to the activities of PLPS (T/H169N) in the presence of glutamine and R5P, PLPS (T/H169N) in the presence of $AmSO_4^{-2}$ and R5P, PdxS in the presence of $AmSO_4^{-2}$ and R5P, and PdxS in the presence of R5P.

Post crystal growth dehydration experiments increase resolution.

Initial crystals of PLPS/H169N$_T$ co-crystallized with glutamine and R5P diffracted to 3.9Å. From this structure I were able to observe partial ordering of the C-terminal tail of PdxS. Density was present for the backbone and I could model the alpha carbons up to residue 290 (Fig. 3.5). Unfortunately, the density was too weak to confidently model the side chains. Confident that a higher resolution structure could be obtained, I attempted post crystal dehydration experiments. The objective was to decrease the